scientific reports

OPEN

3D geothermal model of southern Italy based on the Curie isotherm depth

Maurizio Milano[1]✉, Yemane Kelemework[2], Marina Iorio[3], Mahmoud Ahmed Abbas[1] & Maurizio Fedi[1]

In this study, we build a 3D regional-scale thermal model beneath southern Italy using the Curie isotherm as the bottom boundary condition for the heat-conduction equation. The thermal model is based on solving the 3D steady-state heat conduction equation using a finite-difference approach. Our model consists of five major crustal layers, including the depth to the magnetic basement, the magnetic bottom, and the Moho. For each layer we assigned representative radiogenic heat source and thermal conductivity values based on the average crustal and thermal properties of the study area. The Curie depth, estimated from spectral analysis of aeromagnetic data, is treated as a first-order proxy for the ~580 °C isotherm, and it acts as the model lower boundary. Our model provides a spatially continuous image of the crustal temperature distribution across the Tyrrhenian back-arc basin, the Apennine fold-and-thrust belt, and the Adriatic–Ionian foreland. The results reveal pronounced lateral variations in the crustal thermal regime. Thermal gradients range from ~25 °C/km beneath the Adriatic and Ionian regions to ~75 °C/km beneath the Marsili Basin and Aeolian Arc in the Tyrrhenian Sea where the Curie isotherm is predicted to occur at depths of only 8–10 km. Conversely, the Curie depth is 30–34 km below the Apennine belt and the Calabrian arc, which indicates a much colder and mechanically more resistant crust. Similarly, our estimated heat flow varies from ~40 mW/m² in the Calabrian Arc and the central Apennines, to over 200 mW/m² in the volcanic areas of the south-eastern Tyrrhenian Sea. These patterns reflect the geodynamic evolution of the region, with asthenospheric upwelling and lithospheric thinning occurring beneath the Tyrrhenian retro-arc basin, and thicker, colder lithosphere beneath the orogenic and foreland domains. In addition, our model provides quantitative constraints on the thermal architecture and rheological structure of the lithosphere beneath southern Italy. The predicted temperature field suggests that temperatures of 150–250 °C may be reached at depths of 3–5 km in several sectors of the Tyrrhenian margin and volcanic provinces, indicating favorable conditions for geothermal exploitation where sufficient permeability is present. The proposed framework therefore offers an improved regional baseline for geothermal exploration and for future thermo-mechanical modeling of the central Mediterranean lithosphere.

Keywords Curie Isotherm, Spectral Analysis, Thermal Modeling, Magnetic field, Southern Italy, Heat Flow

Information about the temperature distribution in the crust is paramount to understand the thermal evolution of the Earth at local and global scales, to explore geothermal resources, and to construct basin modeling[1–4]. Near surface heat flow and temperature measurements, along with physical parameters, are mostly used to characterize the temperature variation within the first few kilometers of the Earth[4–7]. To understand deep geothermal systems, surface observations were extended to the deep crust, the Moho, or even the lithosphere, using the heat equation model[5,6,8,9]. To be able to extend near surface thermal data to a greater depth, we need boundary conditions at the sides of the thermal model, and a crustal structure model and associated physical parameters. One of the main criticalities in solving the heat conduction equation is that the bottom boundary condition is unknown[1,8]. Moreover, temperature and heat-flow measurements from boreholes are often unevenly distributed and insufficiently deep, limiting their ability to reliably constrain deep geotherms. One way to partially overcome these limitations is to derive deep thermal constraints from geological and geophysical observations[10]. Common techniques used for this purpose include:

[1]Department of Earth, Environment and Resources Science, University of Naples Federico II, Naples 80126, Italy. [2]Eni S.p.A. Natural Resources, Via Emilia, 1. 20097 San Donato Milanese, Milano, Italy. [3]Institute of Marine Sciences of Naples - National Research Council (ISMAR-CNR), Naples 80133, Italy. ✉email: maurizio.milano@unina.it

- Petrological and geochemical analysis of xenoliths[10–12]: they are useful to determine the thermal structure and composition of the deep parts of the lithosphere.
- Magnetic methods for Curie depth estimation. The inferred Curie isotherm represents valuable information on the thermal property of the lower crust[13–16]. The Curie temperature, 580 °C for magnetite, marks the threshold at which magnetic minerals lose their spontaneous magnetization and become paramagnetic.
- Seismic velocity tomography for velocity-temperature conversion[17,18] and magnetotellurics for upper mantle resistivity estimation[10,19], which are important to infer and interpret fluid-dominated and convective zones[10,18].

Although the geophysical and petrological models suffer from uncertainty, they still can play an important role in constraining deep geotherms. They can substantially supplement near-surface thermal data.

The study area lies within a geodynamically active segment of the Mediterranean, with complex crustal architecture, high heat flow associated with rifting and volcanism, and multiple zones with documented thermal anomalies[20]. These conditions make the region a prime focus for geothermal research with the aim of quantifying subsurface temperature distribution, identifying potential reservoirs, and supporting geothermal energy exploration.

Most of the existing geothermal models of southern Italy are based on surface heat-flow measurements, shallow borehole temperature gradients, and 2D conductive models developed along selected transects across the Apennines belt and the Tyrrhenian Sea margin. The studies produced surface heat-flow maps[2,21,22] and temperature-gradient estimates down to approximately 3 km depth[20,23], based on heterogeneous datasets. These results consistently reveal exceptionally high heat-flow values across the Tyrrhenian domain, progressively decreasing toward the Apennine belt, with particularly steep thermal gradients along the coastal areas. Additional thermal modeling efforts along selected profiles in Southern Italy include the works of Della Vedova et al.[2], Solaro et al.[24], and Tumanian et al.[18], among others. More locally, Castaldo et al.[25] investigated the influence of thermo-rheological properties on surface deformation beneath Ischia Island, while extensive datasets from hot springs, fumaroles, and gas vents, coupled with geochemical analyses, have enabled the development of detailed conceptual models of hydrothermal systems in Southern Italy[26].

More recently further studies have been carried out for the thermal modelling of the local thermal regime in specific sectors of Southern Italy. For instance, Floridia et al.[27] interpreted the present-day conductive thermal field of Sicily through 3D lithospheric-scale gravity modeling, using lithology-dependent physical properties to constrain the thermal structure. Giuffrida et al.[28] developed a 3D hydraulic-thermal model of Pantelleria Island (Sicily Channel), combining steady-state and transient simulations over a 50 kyr timescale and producing temperature distributions validated against well data. Finally, Vespasiano et al.[29] presented a 3D steady-state thermal model of the Calabria region, integrating geological, geophysical, and borehole temperature data within a finite-element modeling framework.

Despite these advances, the deep thermal structure of southern Italy remains weakly constrained, primarily due to the limited depth and uneven distribution of borehole temperature data and to the intrinsic difficulty of defining reliable basal boundary conditions for geothermal models[20,30]. Moreover, previous thermal models typically imposed basal heat flow or Moho-level temperatures inferred from geodynamic assumptions or surface observations[2,18]. These limitations are especially critical in areas such as the Apennine belt and the Calabrian Arc, where low surface heat flow, thick crust, and complex tectonic architecture coexist[2,30].

Consequently, an independent constraint on deep crustal temperatures is essential to reduce model non-uniqueness and resolve the transition between cold orogenic domains and hot back-arc regions. In this study, we use the Curie isotherm depth as a lower boundary condition for a regional 3D steady-state conductive thermal model. This depth model is independently derived from spectral analysis of aeromagnetic data, following established methodologies[13–15]. Because it provides continuous regional coverage and a physically defined temperature reference (~ 580 °C), the Curie depth serves as an effective constraint for the heat equation. Similar approaches have been successfully tested in other geothermal contexts. For instance, Mather and Fullea[31] constrained the geotherm beneath the British Isles using Bayesian inversion of magnetic data, while Guerrero-Martínez et al.[32] applied 3D modeling in the Acoculco caldera to establish background heat flow. Building on these precedents, we assess the applicability of magnetic Curie isotherm estimates as robust boundary conditions within a geodynamically complex setting. There is no guarantee that the estimated magnetic bottom represents the Curie temperature surface[33–35]. However, magnetite is generally assumed to be the dominant magnetic mineral contributing to long-wavelength magnetic anomalies in continental crust[34]. Therefore, we assume that 580 °C is a reasonable Curie temperature for deep crustal rocks.

By integrating Curie depth information with geological, geophysical, and borehole data, we present a comprehensive 3D thermal model of southern Italy. This model quantifies lateral and vertical thermal contrasts across major tectonic domains and characterizes the transition between extensional and compressional regimes. Our results provide a refined understanding of deep regional temperatures, offering a more robust assessment of how tectonic setting, crustal structure, and lithospheric processes jointly control the geothermal potential of southern Italy.

Geological setting and implications for the thermal structure

The Apennine Mountain chain (Fig. 1) extends from northern Italy down to Sicily and represents a complex fold-and-thrust belt formed during the collision of the western continental margin of Adria (the African Promontory) with the Sardinia–Corsica block[36–38]. This mountain chain can be subdivided into two major sectors: the northern–central Apennines and the southern Apennines[36,37,39–44].

The abundance of high-quality geological data, together with extensive hydrocarbon exploration, provides crucial information into the structural architecture and tectonic development of the Apennine belt[37,40–42].

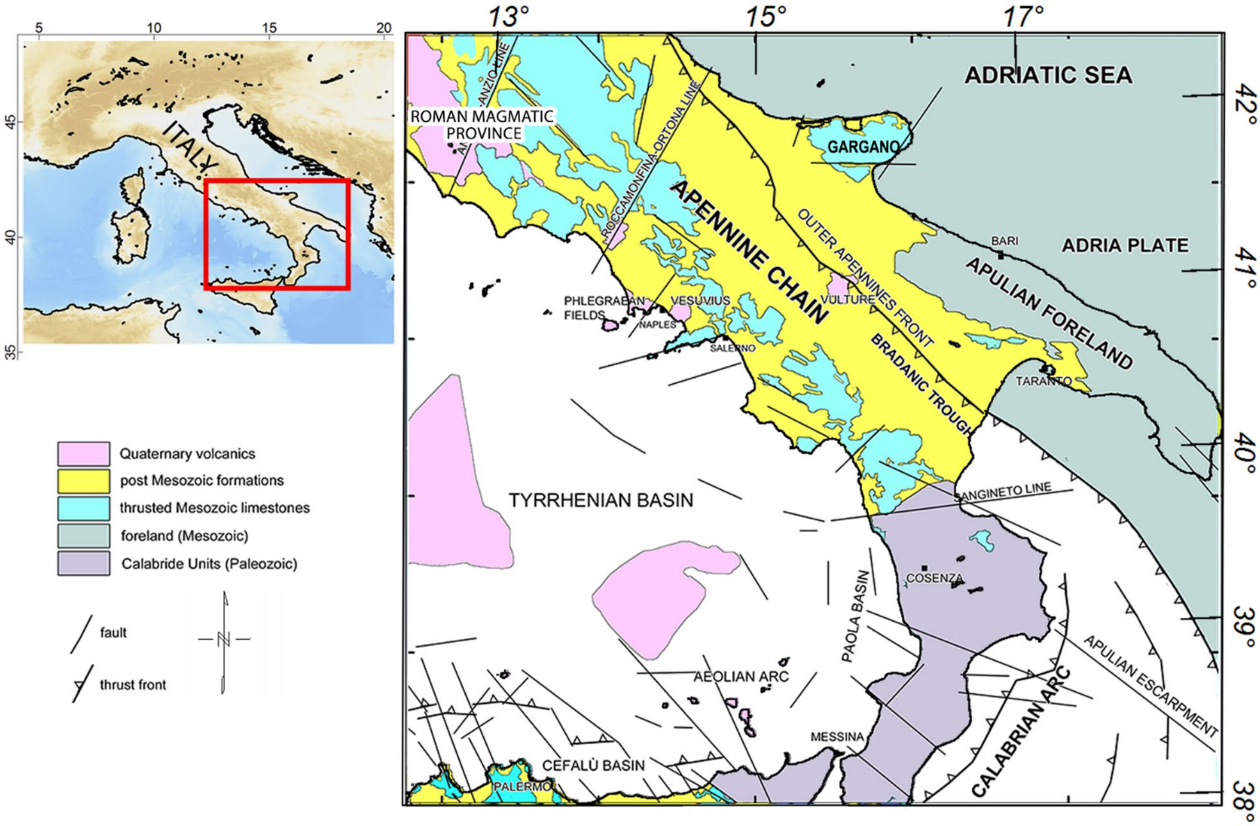

Fig. 1. Simplified geological and structural map of Southern Italy (redrawn after Bosellini[54].

Northern Apennines are mostly dominated by north- and northeast-verging thrusts[42], whereas the central Apennines exhibit north-, northeast-, and east-northeast-verging thrust structures that divide the crust into multiple tectonic slices[42,45]. In contrast, the southern Apennines are mainly defined by east-northeast- and east-verging duplex structures and out-of-sequence thrust faults[42,46]. The geodynamic processes driving the evolution of the Apennines produced an eastward migration of the subduction hinge, along with the associated accretionary wedge and back-arc basin[47]. The tectonic accretion of the Tyrrhenian-Apennines system began in the middle Miocene and produced simultaneously extensional tectonics along the Tyrrhenian margin and progressive reduction on the foreland side of the orogen[37,47–50].

The Tyrrhenian back-arc basin consists mainly of partly oceanic and thinned continental crust with an irregular seafloor[37,39,41,42,50,51] as result of the E-W-opening and the stretching mechanisms. It follows that the extensional thinning of the lithosphere allowed the formation of two large bathyal basins (Vavilov and Marsili basins) and several Pliocene-Pleistocene volcanic edifices along the peri-Tyrrhenian margin[39,42,52]. The Southern Apennines orogenic belt is mostly characterized by allochthonous oceanic nappes of Tethyan derivation overlying continental nappes from the Adria plate[53] (Fig. 1). Such a multilayer complex consists mostly of the Apulian platform followed by the Lagonegro-Molise basins, the Apennine carbonate formation and the Liguride-Sicilide basinal provinces[41].

Geophysical investigations conducted along the Apennine chain have significantly improved our understanding of the crustal architecture and its physical properties. Seismic imaging and potential-field analyses indicate that the Moho boundary deepens from more than ~ 40 km beneath the northern Apennines to approximately 35 km beneath the central and southern Apennines (Fig. 2a)[37–41]. In contrast, the crust is considerably thinner in the Tyrrhenian domain, where Moho depths reach about 10 km beneath the Vavilov and Marsili basins in the southeastern Tyrrhenian Sea and increase to ~ 20–25 km beneath western Tuscany and Latium[37,38,41,42]. Further east, Moho depths of roughly 30 km characterize relatively stable regions such as the Adriatic domain, and the Apulian foreland[15,55–57].

This marked variability in crustal thickness reflects the complex geodynamic evolution of the central Mediterranean and exerts a strong control on the geothermal framework of southern Italy. In particular, the interaction between the Apennine orogenic system and the Tyrrhenian back-arc basin plays a fundamental role in shaping the regional thermal regime. The opening of the Tyrrhenian Sea, associated with eastward rollback of the subducting Adriatic–Ionian slab, promoted lithospheric thinning, mantle upwelling, and widespread magmatic activity along the Tyrrhenian margin[58,59]. Consequently, heat-flow maps and previous geothermal studies reveal a pronounced thermal asymmetry across the region (Fig. 2b), with very high heat-flow values in the Tyrrhenian domain that progressively decrease toward the Apennine belt and the Adriatic–Ionian foreland[2,21,22]. These contrasts are commonly interpreted as the thermal expression of enhanced mantle

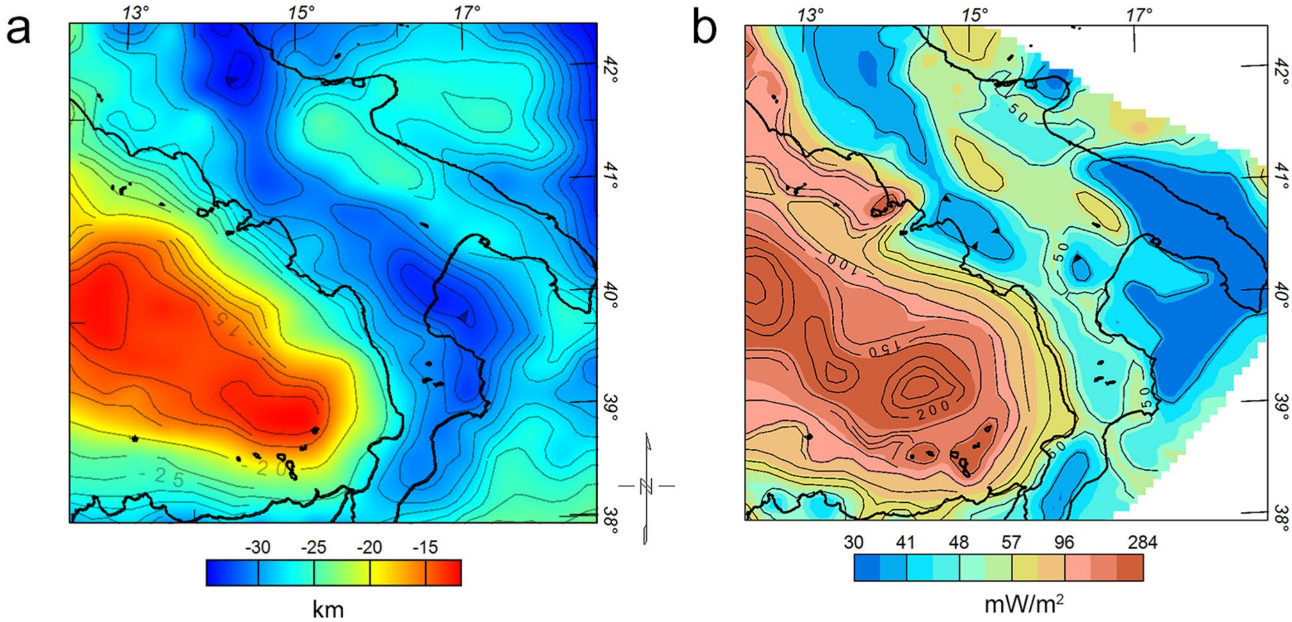

Fig. 2. (**a**) Moho depth map derived from gravity data (modified after Kelemework et al.[55]; (**b**) Observed heat flow digitized from the Geothophica database[23].

heat input and asthenospheric upwelling beneath the back-arc basin, compared with the colder and thicker lithosphere underlying the orogenic belt and foreland sectors[18,30].

Structural and tectonic features further modulate the regional geothermal pattern. Extensional fault systems, crustal thinning, and Quaternary volcanic districts in Campania and along the southern Tyrrhenian margin favor high heat flow and active hydrothermal circulation[60]. Conversely, thrust structures, crustal thickening, and deep groundwater circulation within the carbonate platforms of the Apennines tend to reduce surface heat-flow values by redistributing heat through advective processes[61]. In addition, major fault zones and fracture networks may act as preferential pathways for deep CO_2-rich fluids rising from the mantle and lower crust, enhancing advective heat transport and locally amplifying geothermal anomalies[62–64]. The structural architecture of the Apennine belt, including thrust vergence, nappe stacking, and the kinematic evolution of the orogenic system[40,42] may therefore influence the thermal field indirectly by controlling crustal thickness, radiogenic heat production, permeability distribution, and fluid circulation pathways, rather than through structural geometry alone[10,19].

Methodology

Spectral analysis for depth estimation

Depth to the Curie point (CPD) can be calculated using spectral analysis of magnetic data or forward modelling of magnetic data. The spectral method is the most commonly used one and its mathematical formulation is based on either a statistical ensemble of blocks[15,65,66] or random uncorrelated sources[13,67] or even random fractal noises[14,68,69].

In this study we consider the statistical block ensemble approach[65,66] where the ensemble average $\langle E(k,\theta)\rangle$) of the magnetic anomaly is expressed by:

$$\langle E(k,\theta)\rangle = 4\pi^{2}\overline{J}^{2}\langle e^{-2hk}\rangle\langle T^{2}(k)\rangle\langle S^{2}(k,\theta)\rangle\langle R_{T}^{2}(\theta)\rangle\langle R_{M}^{2}(\theta)\rangle \tag{1}$$

where: $k=\left(k_x{}^2+k_y{}^2\right)^{1/2}$ is the wave number, h is the depth; $\theta = \tan^{-1}(k_x/k_y)$; $R_T^2(\theta) = \left[n^2 + (l\cos\theta + m\sin\theta)^2\right]$; $R_M^2(\theta) = \left[N^2 + (L\cos\theta + M\sin\theta)^2\right]$, $\langle T^2(k)\rangle = \langle (1-e^{-tk})^2\rangle$ is the thickness factor and $\langle S^2(k,\theta)\rangle$ is a factor related to the source lateral dimension. L, M, N are the magnetization direction cosines and (l, m, n) the geomagnetic field vector direction cosines.

We may compute the radial spectrum by taking the radial average of $\langle E(k,\theta)\rangle$:

$$\langle \overline{E}(k)\rangle = 4\pi^{2}\overline{J}^{2}\langle e^{-2hk}\rangle\langle T^{2}(k)\rangle\langle S^{2}(k)\rangle\langle R_{T}^{2}\rangle\langle R_{M}^{2}\rangle \tag{2}$$

where $\langle S^2(k)\rangle = \frac{1}{\pi}\int_0^{\pi}\langle S^2(k,\theta)\rangle d\theta = k^{-2.9}$.

From Eq. 2, it has been noted that only the factors $\langle e^{-2hk}\rangle$, $\langle T^2(k)\rangle$, $\langle S^2(k)\rangle$ affect the shape of the logarithm of the radial spectrum[65,66].

Therefore, we can infer the depth to the magnetic top $\bar{h}$, by reducing Eq. 2 to:

$$ln(\langle \overline{E}(k) \rangle) \approx ln(A) - 2k\,\bar{h} \quad (3)$$

where $A = 4\pi^2 \bar{J}^2 \langle R_T^2 \rangle \langle R_M^2 \rangle k^{-2.9}$[15,66].

The depth to the magnetic top is determined by analyzing segments of the spectrum in which the logarithm of the power spectrum exhibits an approximately linear trend, following the classical methodology for spectral analysis of potential fields[65]. It is also important to note that the statistical block ensemble can be interpreted in either a single-ensemble or double-ensemble framework. In the single-ensemble case, a linear regression is fitted to the appropriate linear segment of the spectrum to estimate the depth to the top (e.g., Fig. 1 in Kelemework et al.[15]), as emphasized by Spector and Grant[65]. However, in the case of the double ensemble, it can be identified by a change in slope of the power spectrum, which indicates the presence of ensemble sources at different depths. For this case, the depth to the deep source can be estimated by drawing a linear regression to the small wavenumber part of the spectrum (note that the range of wavenumber depends on the linear part of the spectrum), whereas the shallower sources can be estimated by drawing a slope to appropriate intermediate-high wavenumber sectors of the spectrum. The case of a double ensemble has been shown by Spector and Grant[65] (their Figures 4b and Figure 5b), and by Fedi et al.[66] (their Figure 8 and Figure 9).

The next step is to infer the depth to the magnetic bottom. This task is more challenging and different spectral techniques have been developed: the spectral peak method[15,70,71] the centroid method[13,15,72] the nonlinear curve fitting method[14,68] the forward modelling of the spectral peak method[34,73] and the de-fractal method[74].

For estimating the centroid depth $\bar{h}_0$, Eq. 2 reduces to:

$$ln(\langle E(k) \rangle) \approx ln(P) - 2k\bar{h}_0 \quad (4)$$

where $P = \frac{64}{3}\pi^2 \bar{J}^2 \langle R_T^2 \rangle \langle R_M^2 \rangle \bar{d}^2 \; k^{-0.9}$ [15].

Depth to the centroid is estimated by fitting slope to the linear very low wavenumber part of the radially average power spectrum.

The depth to the magnetic bottom can then be easily derived from the depth to the top and centroid as follows[13]:

$$h_b = 2\,\bar{h}_0 - \bar{h} \quad (5)$$

where h_b is depth to the bottom.

Models of the depth to the top and bottom of magnetic sources

We inferred the depth to the top and bottom of magnetic sources in Southern Italy using the aeromagnetic dataset of Italy, collected during the 1970 s and 1980s[75,76], (Fig. 3a). The aeromagnetic data were compiled from different ground, onshore and offshore aeromagnetic surveys that have been merged onto a draped surface 1 km above the topography and gridded with a 1 km sampling interval. In this study, we applied a draped-to-level upward continuation to a constant altitude of 3 km a.s.l[77]., utilizing the wavelet-based algorithm developed by Ridsdill-Smith[78].

Following Kelemework et al.[15], here we used a 80 × 80 km^2 window size in the Tyrrhenian Sea, where seismic study indicates an expected depth to the bottom of around 10–20 km and a 100 × 100 km^2 window size in the Apennines area, where the expected depth to the bottom is around 30 km, (for details about the choice of the window size see Kelemework et al.[15,55]). Representative power spectra used to derive the depth to the top (Eq. 3), and the centroid (Eq. 4) are presented in Fig. 3a and b. Error bars correspond to the 95% confidence intervals of the radial average of the power spectrum. The resulting depth estimates from individual windows were interpolated to obtain continuous maps of the upper and lower boundaries of magnetic sources.

Figure 4a and b present the inferred models of the top and bottom of magnetic sources across Southern Italy. The magnetic top lies at less than 2 km depth in the Tyrrhenian sector, deepening to roughly 14 km below the fold-and-thrust belt and the Calabrian Arc, and reaching about 12 km beneath the Apulian foreland and the Adriatic margin (Fig. 4a). Shallow magnetic-top depths also appear beneath and in the vicinity of Mount Vulture, as well as along the Gulf of Naples.

The magnetic bottom spans from approximately 8 km beneath the Tyrrhenian crust to over 34 km beneath the Apennine chain (Fig. 4b). The comparatively shallow magnetic-bottom depths mapped under the Tyrrhenian Sea and the NW Campania coastline coincide with an area represented by exceptionally high heat flow, exceeding 200 mW/m^2 [2].

In the hanging wall of the Apennines, the magnetic bottom surface lies at roughly 28 km depth within the southern Calabrian Arc, increasing to nearly 33 km both to the north and south[55]. These depths are consistent with the generally low heat-flow regime of the region, which varies between about 30 and 50 mW/m^2 [2,56]. A notably shallow magnetic-bottom depth appears in the Mt. Vulture area, following a marked north–south alignment that coincides with elevated heat-flow values (Fig. 2b).

Our estimates place the basal magnetic surface at 26–32 km beneath the southern Adriatic basin and, moving toward the Ionian basin, at approximately 34 km under the frontal sector of the Calabrian Arc and around 20 km

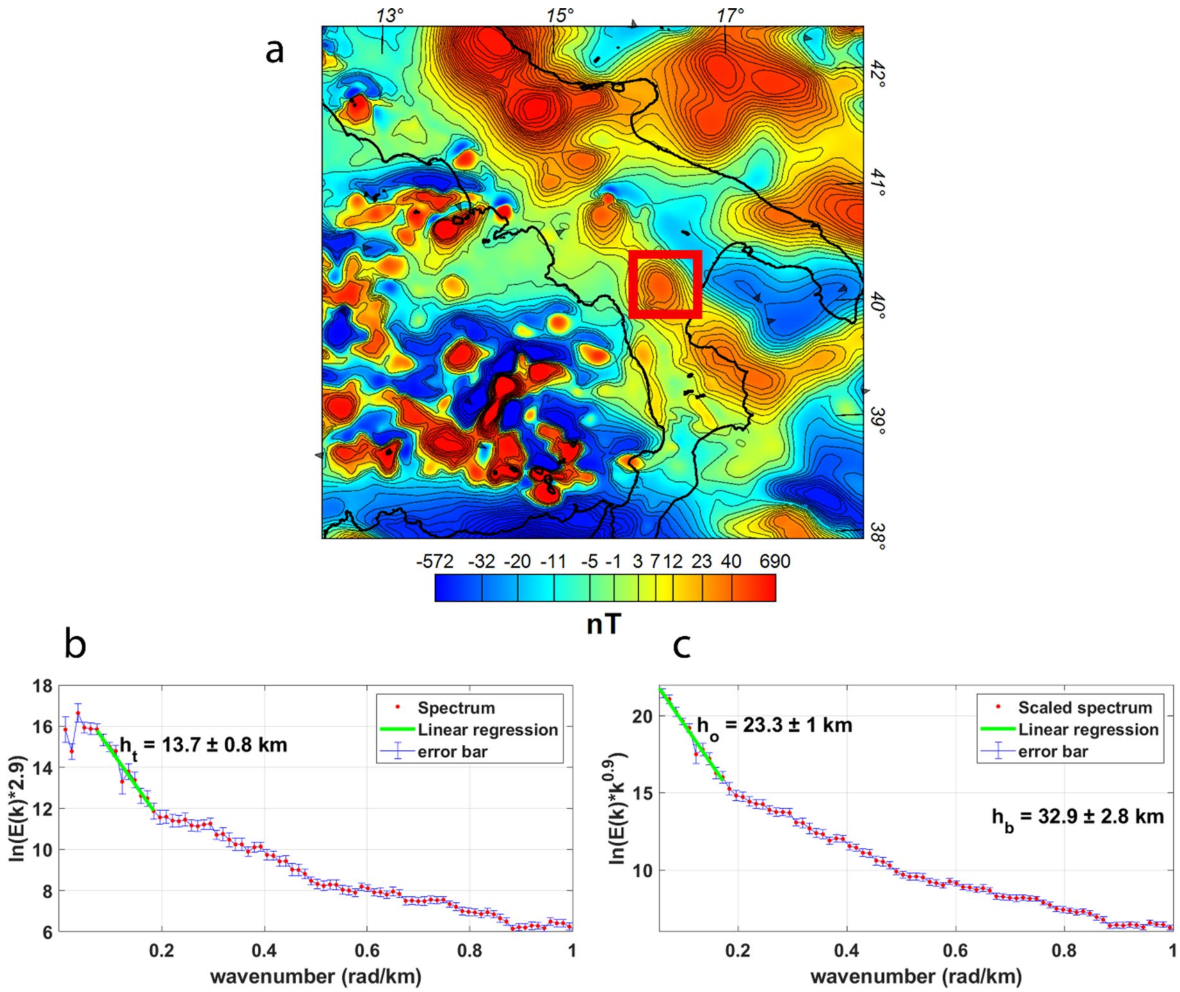

Fig. 3. Aeromagnetic map of Italy (**a**) and power spectra for estimating the depth to the top (**b**) and the depth to the centroid (**c**) for the window located by red box on (a).

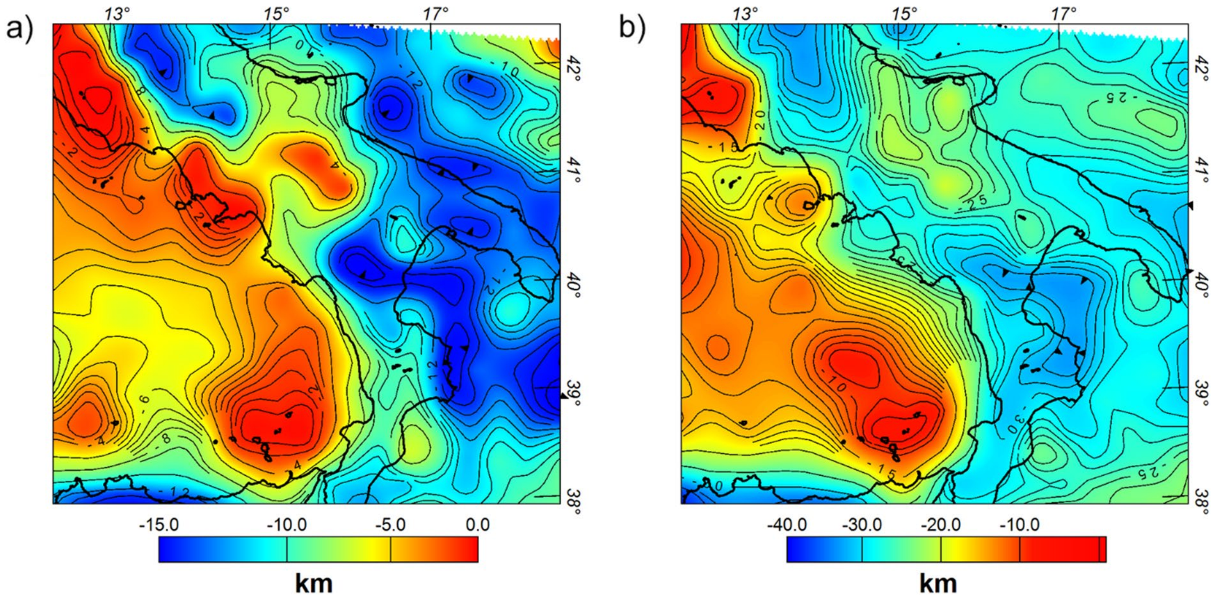

Fig. 4. Depth to the top (**a**) and bottom (**b**) of the magnetic sources estimated from the spectral analysis of the aeromagnetic field dataset in Fig. 3a.

beneath the Calabrian accretionary wedge. The very low heat flow here (30–40 mW/m²) has been linked to the presence of old oceanic lithosphere[56,79–83].

In this work, we treat the depth to the magnetic bottom as a proxy for the Curie isotherm, which defines the lower thermal boundary for the heat-conduction model. Characterizing the crustal structure is also essential for assigning realistic thermal conductivity and heat-production parameters, and it can be constrained through seismic data, potential-field analyses, and geological interpretation.

It is important to note that the inferred magnetic bottom does not necessarily coincide with the Curie depth. The disappearance of crustal magnetization may be controlled not only by temperature, but also by lithological variations in the magnetic mineral assemblage[83]. For instance, a strong correlation between the depth of the magnetic bottom and the Moho may indicate that the base of the magnetic layer is primarily governed by compositional contrasts at the crust–mantle boundary[13,83–85]. In contrast, when the magnetic bottom depth correlates with heat-flow variations, it is commonly interpreted as reflecting the Curie isotherm[13,18,85,86].

Numerous studies have demonstrated that, at regional scales, the magnetic bottom derived from spectral analysis often shows good agreement with independent thermal indicators[13,72,74]. This suggests that temperature exerts a primary control on the disappearance of crustal magnetization over large spatial scales. Accordingly, the magnetic bottom is widely used as a first-order approximation of the Curie isotherm in regional geothermal and lithospheric thermal studies. However, this interpretation should be considered thermally meaningful mainly at regional scales, as local discrepancies between the magnetic bottom and the true Curie depth may arise from lateral variations in crustal composition or magnetization.

In the case of southern Italy, we observe a broadly consistent spatial relationship between the depth of the magnetic crustal bottom (Fig. 4b) and the heat-flow distribution (Fig. 2b). At the regional scale, both datasets reveal shallow Curie depths and high heat flow beneath the Tyrrhenian Sea and volcanic provinces, and significantly greater depths associated with low heat flow beneath the Apennines and the Adriatic–Ionian foreland. For clarity, Fig. 5 also presents a direct comparison at selected locations between the CPD and observed heat-flow data. Theoretical curves corresponding to different thermal conductivities are included. Despite some local mismatches, likely due to the differing spatial resolution of well data and the magnetic field–derived CPD model, a general inverse relationship is evident, with high heat-flow values corresponding to shallow Curie depths, and vice versa. A reasonable agreement is obtained for $k = 2.5$ W m^{-1} ºC^{-1} over the Apennines and $k = 3$ W m^{-1} ºC^{-1} over the Tyrrhenian region.

A key aspect of the analysis is the comparison between the CPD and the Moho depth model. In Fig. 6a, we present the statistical distribution of the difference between the two surfaces (CPD – Moho). The histogram shows that most values cluster around positive differences, indicating that, on average, the magnetic bottom lies within the crust. This is consistent with the expectation that the Curie isotherm is generally reached before the crust–mantle boundary.

A comparison with the spatial patterns of the two models (Figs. 2a and 3b) further confirms that the CPD is predominantly shallower than, or comparable to, the Moho depth, particularly in correspondence with volcanic provinces and thermally anomalous regions of the southern and northern Tyrrhenian domain. This observation agrees with the presence of elevated geothermal gradients in these areas.

However, the distribution also exhibits a non-negligible tail toward negative values. These cases, where the CPD appears deeper than the Moho, are mainly observed in the Ionian Sea, the central Apennines, and the Calabrian Arc. However, these discrepancies must be interpreted with caution, especially since the difference is small and they fall within the uncertainty of the method.

For this reason, Figs. 6b–d provide a comprehensive assessment of the uncertainties associated with the estimated depths of the magnetic top, CPD, and Moho. These uncertainties are computed following the approach of Kelemework et al.[15], accounting for the combined effects of spectral analysis and the linear regression used, both used in the depth estimation process. For each model, we present both the statistical distribution (histograms) and their spatial variability (maps), allowing for a more robust illustration of the reliability of the results.

In Fig. 6b, the uncertainty associated with the magnetic top depth is shown. The distribution is positively skewed, with a mean of approximately 570 m and a standard deviation of about 250 m. Most values range between ~ 300 and ~ 700 m, although a limited tail extends beyond 1 km. This pattern likely reflects the sensitivity of shallow magnetic sources to high-frequency noise, window size selection, and spectral resolution limitations.

Figure 6c illustrates the uncertainty distribution for the CPD. As expected, these uncertainties are significantly larger than those of the magnetic top, with a mean of ~ 2 km and a standard deviation of ~ 630 m. The distribution is broader and right skewed, with most values falling between ~ 1.5 and ~ 2.5 km. This increased uncertainty highlights the intrinsic difficulty in resolving deeper magnetic boundaries, as long-wavelength anomalies are more affected by regional trends.

Finally, Fig. 6d presents the uncertainty associated with the Moho depth model. The distribution is comparable in magnitude to that of the CPD, with uncertainties generally ranging between ~ 2 and ~ 4.5 km. The spatial pattern reveals that higher uncertainties are concentrated in tectonically complex regions, such as the southern Apennines and the Calabrian Arc, where crustal structure is highly heterogeneous. Despite this, the overall uncertainty remains acceptable for regional-scale interpretations and consistent with the depth of the investigated structures. Importantly, these uncertainty estimates are propagated into the thermal modelling, allowing us to define realistic uncertainty envelopes for the derived geotherms.

It is worth noting that, areas where the CPD lies at a greater depth than the Moho and where the difference between the two exceeds the sum of their respective uncertainties may indicate the presence of a magnetized upper mantle. This behaviour can be attributed to specific lithospheric conditions, such as a relatively cold thermal regime and/or mantle serpentinization, particularly in the Ionian Arc and Calabrian Arc regions[84,85].

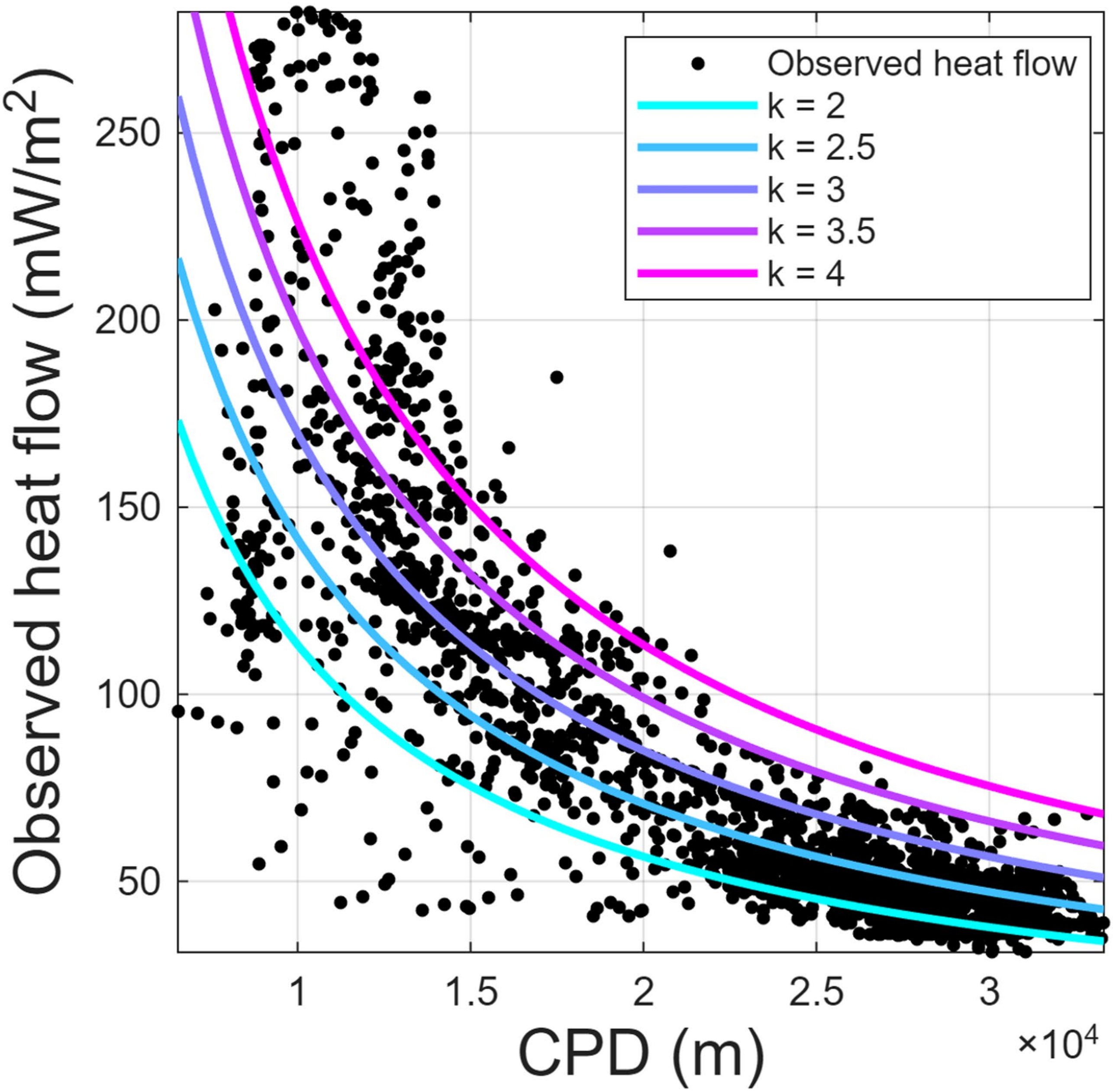

Fig. 5. Comparison between the observed heat flow and CPD. Heat flow assuming different thermal conductivities are also shown.

Overall, although local lithological variations may influence the depth of the magnetic bottom, the observed consistency between CPD, heat-flow distribution, crustal thickness, and regional geodynamic setting suggests that, at the scale of southern Italy, the magnetic bottom is primarily controlled by temperature. This supports its use as a reliable proxy for the Curie isotherm in regional thermal modelling.

3D heat conduction

Heat transport in the lithosphere occurs through conduction, convection, or advection. In geodynamically stable settings, conduction is the prevailing mechanism, while advective heat transfer is characteristic of regions experiencing active deformation[2,10,86]. The convective heat transfer mechanism plays an important role in the mantle. It may also be important in near-surface convective thermal systems, volcanic regions, and areas dominated by ground water circulation.

Assuming the conduction heat transfer mechanism, the temperature distribution within the lithosphere corresponds to its values $T\,(x, y, z, t)$, where x and y denote the horizontal location of a point, z is the depth and t denotes time. In three dimensions (3D), the heat conduction equation can be written as[87]:

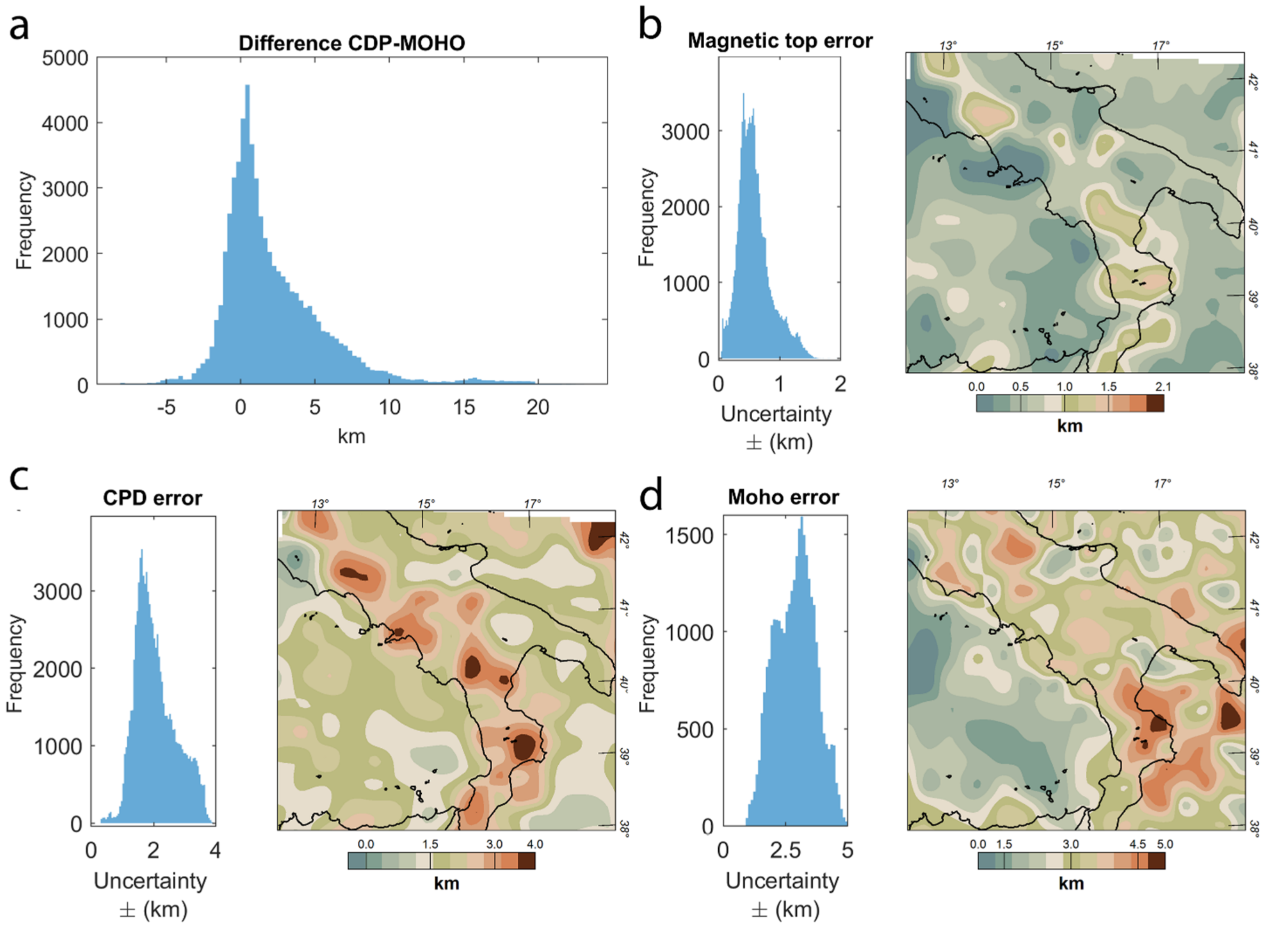

Fig. 6. Results of the uncertainty analysis. **a**) Comparison of the Moho depth map and the estimated CPD. Statistical analysis of the model uncertainty and their maps for the depth to the top (**b**), CPD (**c**) and the Moho (**d**).

$$\rho\,(x,y,z)c_p(x,y,z)\frac{\partial\,T\,(x,y,z,t)}{\partial\,t} = \frac{\partial}{\partial\,x}\left(k\,(x,y,\,z)\,\frac{\partial\,T\,(x,y,\,z,t)}{\partial\,x}\right) + \frac{\partial}{\partial\,y}\left(k\,(x,y,z)\,\frac{\partial\,T\,(x,y,z,t)}{\partial\,y}\right) + \frac{\partial}{\partial\,z}\left(k\,(x,y,z)\,\frac{\partial\,T\,(x,y,z,t)}{\partial\,z}\right) + A_p(x,y,z,t) \quad (6)$$

where T is the temperature, $\rho\ (x, y, z)$ is the rock density, $c_p\ (x, y, z)$ is the specific heat capacity, $k\ (x, y, z)$ is the thermal conductivity, and $A_p\ (x, y, z)$ is the rate of internal heat production per unit volume. For a steady-state heat conduction, Eq. (6) reduces to:

$$\frac{\partial}{\partial\,x}\left(k\,(x,y,\,z)\,\frac{\partial\,T\,(x,y,\,z)}{\partial\,x}\right) + \frac{\partial}{\partial\,y}\left(k\,(x,y,z)\,\frac{\partial\,T\,(x,y,z)}{\partial\,y}\right) + \frac{\partial}{\partial\,z}\left(k\,(x,y,z)\,\frac{\partial\,T\,(x,y,z)}{\partial\,z}\right) + A_p\,(x,y,z) = 0 \quad (7)$$

Equation (7) constitutes a well-posed boundary-value problem, provided that the surface temperature (T_o) and either the Curie temperature (T_{cpd}) or heat-flow at the bottom of the model are specified[8].

Boundary conditions

Depending on the availability of constraints, different boundary conditions can be used to solve Eq. (2.2). In this study, we use a constant average onshore temperature (15 °C) and offshore sea bottom temperature (13 °C) at the top of the model, Curie temperature (580 °C) at the Curie depth point and thermal insulating conditions along the sides of the model (zero heat flux).

Discretization

The partial differential Eq. (2.2) may be discretized by various methods, including the finite difference method (FDM), the finite element method (FEM) and the finite volume method (FVM). In this paper, we use FDM[88,89] where the discretized finite difference method leads to a linear system of equations which can be written as:

$$\mathrm{AT} = \mathrm{d} \tag{8}$$

where **A** is kernel matrix, **T** is a vector that contains the temperature values at the discrete points (unknown values) whereas the right-hand side **d** is a vector that contains the heat production at discrete points ($\mathbf{A_p}$). Note that the vector **d** also includes the boundary conditions (i.e., $T_1 = T_0$ where T_0 is the surface temperature, $T_b = T_{cpd}$ where T_{cpd} is the Curie temperature).

Solving the linear system of problem

Matrix **A** is large and sparse, and thus an iterative method is more appropriate to solve such linear system of equations [88–90]. Furthermore, because the system is large and sparse, it is advisable to use a preconditioner, which transforms the matrix **A** to accelerate the convergence of the iterative method[90]. Then, Eq. (8) becomes:

$$\mathrm{M}^{-\mathbf{1}}\mathrm{AT} = \mathrm{M}^{-\mathbf{1}}\mathrm{d} \tag{9}$$

where $\mathbf{M}^{-1}$ is a preconditioner, that is an approximation to $\mathbf{A}^{-1}$. Since $\mathbf{M}^{-1}\mathbf{A}$ has a smaller condition number than **A**, the linear system can be solved quickly by iterative methods[90,91]. In this study, we adopt the incomplete LU factorization (ILU) of matrix **A** to form a preconditioner. The incomplete LU factorization is based on computing a sparse lower triangular matrix **L** and a sparse upper triangular matrix **U**. We then solve the linear system using the generalized minimum residual (GMRES) method[92], which is appropriate to solve nonsymmetric coefficient matrix. We use MATLAB to solve the system.

Existence, uniqueness and convergence

Equation (2.4) is a well-posed problem. The problem has a unique solution that depends on the boundary condition (i.e., Curie temperature isotherm) and varies as a function of it. However, uncertainties that arise from computing the depth to the Curie point propagates also into the thermal model. The curvature of the geothermal gradient depends on the heat source and thermal conductivity of the crust. We use a tolerance of $1e^{-6}$ as a convergence criterion.

Crustal and physical models

Crustal model

To characterize the crustal properties and the associated distribution of heat sources, we employed models derived from magnetic data using spectral analysis techniques. Specifically, we utilized the depth-to-magnetic-basement and Curie isotherm models shown in Fig. 4, along with the Moho depth model previously estimated by Kelemework et al.[55] and presented in Fig. 2a.

Based on these models, the vertical geological sections are subdivided into five principal units. The first unit represents the domain of carbonate units and Quaternary sediments between the surface and the top of the magnetic sources (Fig. 7). The second one represents the magnetic crust, spanning from the magnetic basement top to basement bottom (i.e., the Curie depth); this layer largely corresponds to the middle and lower crust. The third unit is defined as the non-magnetic crust, located between the base of the magnetic crust and the Moho discontinuity. The fourth corresponds to a hypothetical magnetized portion of the mantle, defined as the interval located below the Moho and above the base of the magnetic layer. This layer is only identified in limited areas, as its apparent thickness may fall within the uncertainty associated with the CPD and Moho depth models (see Sect. 1.1). The fifth unit below the Moho is part of the upper mantle (Fig. 7).

Thermal conductivity

The thermal conductivity is a transport property difficult to define within the crust. Compilation of thermal conductivity values from different rock samples at room temperature show an average value of 3.0 W/mK for the upper crust, 2.6 W/mK for the lower crust and 3.5 W/mK for the lithospheric mantle[5,93]. However, the variation of thermal conductivity within the lithosphere is generally controlled by its temperature, composition and pressure and different approaches have been proposed for its computation[5,12,93,94].

In this study, we first attempted to get insight into the thermal conductivity distribution from measured data collected in the Southern Apennines[23,95], (Fig. 8a). In the top 3 km, the thermal conductivity varies from 1.4 W/m°C to 2.5 W/m°C, with average value of 2.2 W/m°C (Fig. 8a). However, as one may infer from the figure, the thermal conductivity values seem to increase with depth. We then tried to get additional information from previous studies as well. Della Vedova et al.[2], for example, used thermal conductivity values ranging from 1.8 W/m°C for clays with sands to 3.7 W/m°C for limestone and dolomites. They built a thermal model down to 10 km depth along a profile running from the Tyrrhenian coastline to the Adriatic Sea, with an average value of 2.6 W/m°C. Carlino[60] used an average value of 1.5 W/m°C, assuming this value as representative of the Campania plain. Solaro et al.[24] used different thermal conductivity values, i.e., 2 W/m°C for volcanites, 2.8 W/m°C for limestone, 3.7 W/m°C for dolomite, 1.8 W/m°C for clay-sand, (with an average value of 2.6 W/m°C for the upper crust), 2.5 W/m°C for the lower crust and 3.5 W/m°C for the upper mantle. Tumanian et al.[18] built a thermal model along several profiles using a thermal conductivity value of 2 W/m°C for the sediment, 2.7 W/m°C for the upper crust, 2 W/m°C for the lower crust and 4 W/m°C for the upper mantle. Thus, based on the literature review and the data shown in Fig. 8a, we use an average value of 2.2 W/m°C in the first 3 km, 2.8 W/m°C for the carbonate platforms above the basement, and 2.6 W/m°C for the magnetic crust. Apart from the Tyrrhenian Sea, we assume a thermal conductivity of 2.5 W/m°C below the Curie and above the Moho. In the Tyrrhenian Sea, we assume a constant thermal conductivity of 3.5 W/m°C (Fig. 8b), comparable to the values used by Trumpy and Manzella[23] and Solaro et al.[24].

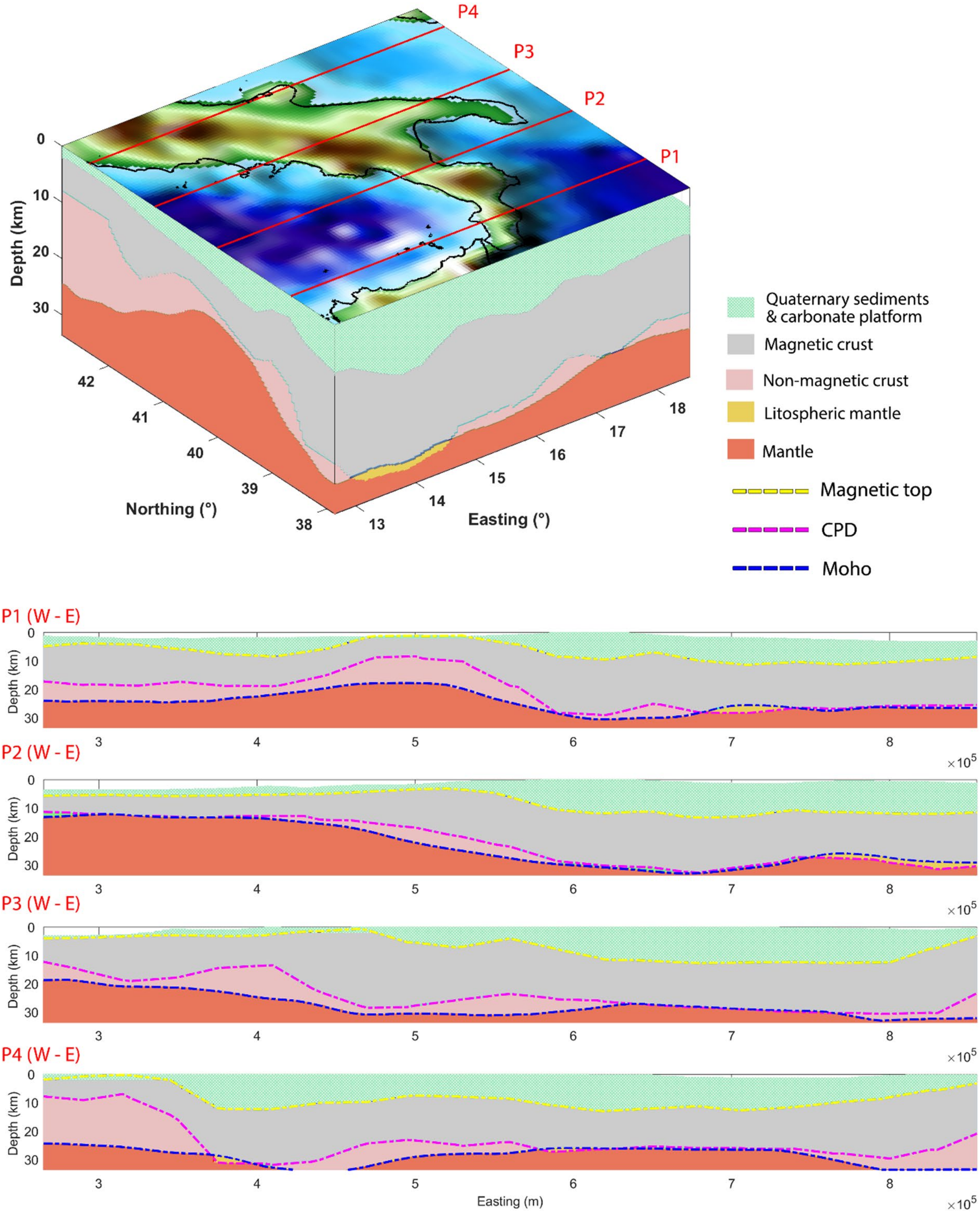

Fig. 7. 3D crustal model and 2D sections extracted along profiles. This model is used to assign the radiogenic heat source and thermal conductivity models.

Heat production

Information regarding the variation of heat production with depth is important for geothermal modeling. It controls the geotherm curvature. The heat production within the crust varies depending on the concentration of radioactive elements, which in turn depends on rock types. The distribution of heat production can be modeled as a function of depth by adopting different assumptions:

(i) heat-production decreasing exponentially within the upper crust;

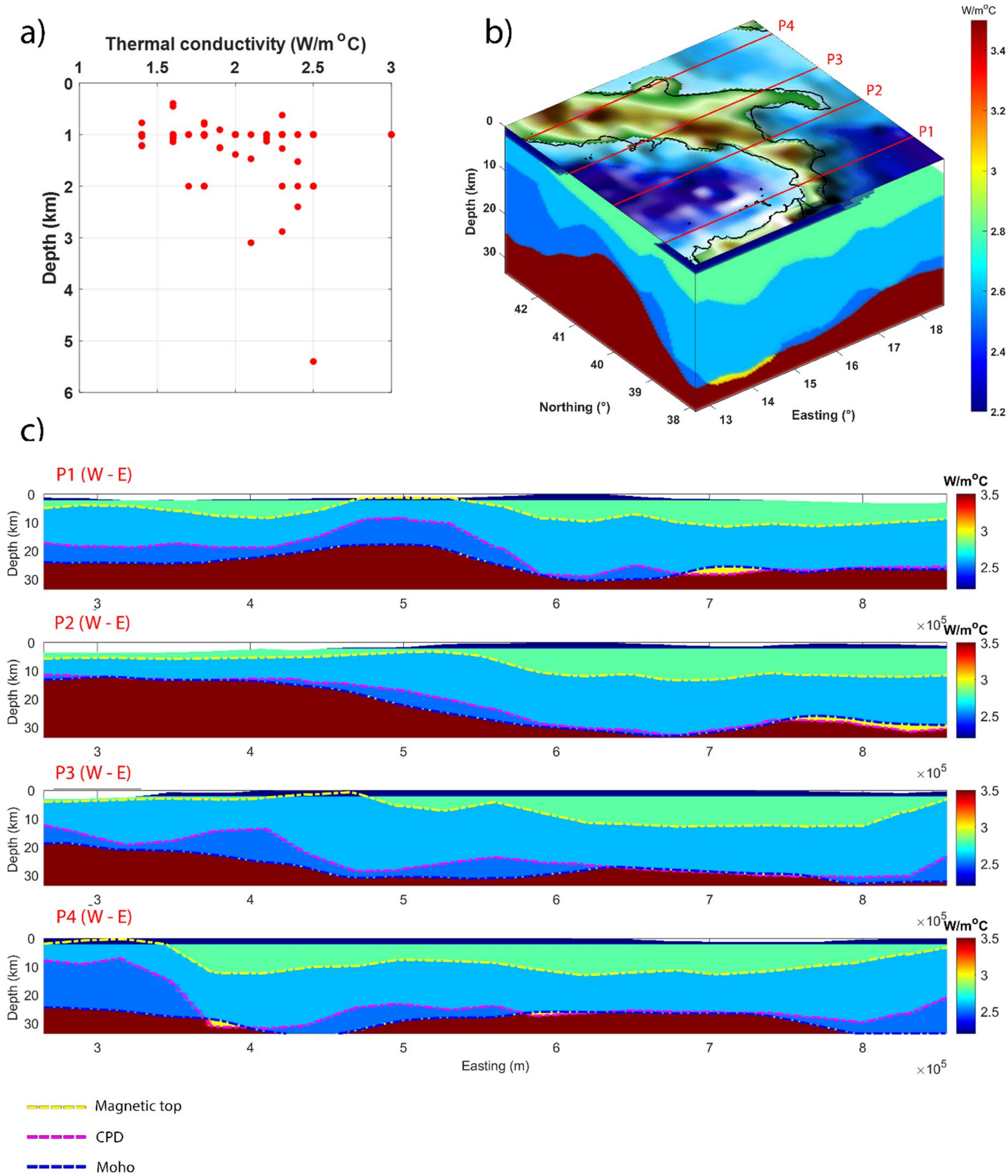

Fig. 8. (**a**) Examples of measured thermal conductivity (data from Geothopica[23]; (**b**) 3D thermal conductivity model and **c**) 2D sections extracted from the 3D model.

(ii) each model layer with constant heat production;
(iii) heat-production decreasing exponentially within each layer.

As for thermal conductivity, there is no simple functional relation that describes the heat production variation vertically and laterally. In the Apennines, the heat production of the carbonate rocks is estimated to vary from 0.04 to 1.6 μW/m^3 (e.g., Carlino[60] and references therein). However, due to the existence of different rock types, it is still challenging to understand the variation of heat production. For that matter, different values have been used by different authors. For the upper crust an average value of 1 μW/m^3 considered by Della Vedova et al.[2]. Tumanian et al.[18] used an average value of 0.8 μW/m^3 for the sediment, 0.9 μW/m^3 for the upper crust, 0.2 μW/m^3 for the lower crust and 0.01 μW/m^3 for the upper mantle.

Here, we assume a constant value of 0.8 μW/m³ in the top 3 km and 1.0 μW/m³ for the carbonate platforms and Quaternary volcanics and an exponential heat production in the magnetic crust: $A_p(z) = 3 * e^{(-z/D)}$, where $D = 10$ km is the average thickness of the heat producing layer, similar to the model adopted by Santini et al.[96]. We assume a constant heat production of 0.01 μW/m³ in the upper mantle as derived from geochemical analysis of xenolith samples[12] (Fig. 9).

Results

Thermal model

Figure 10 presents the 3D thermal distribution of the Southern Apennines, constrained by the Curie depth, along with horizontal temperature slices at 1 km, 2 km, 3 km, and 4 km depth. The computed crustal temperature

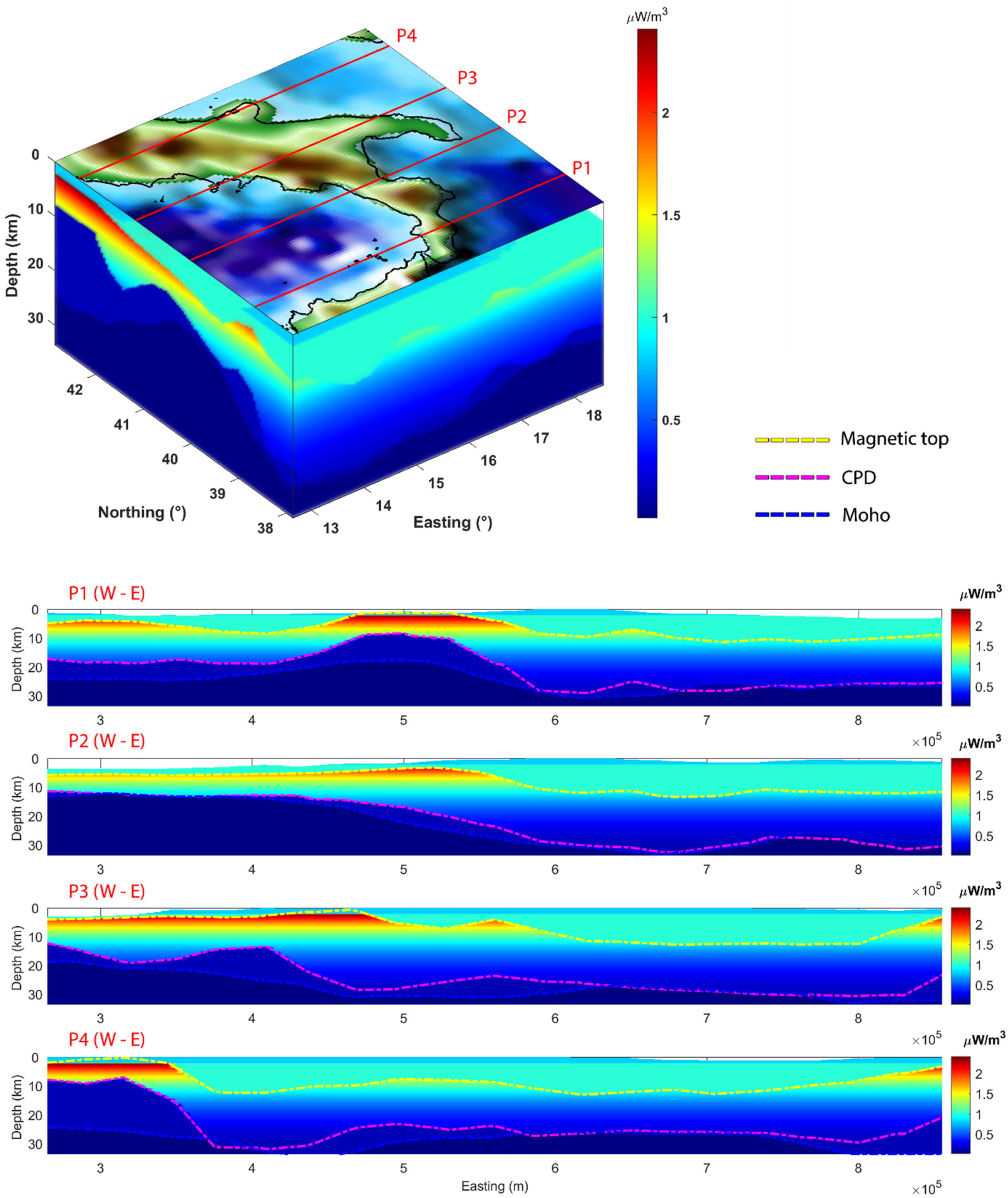

Fig. 9. 3D crustal heat production model and extracted sections.

patterns appear to reflect the volcano-tectonic development of the region as well as the physical properties of the lithosphere. In Fig. 11 we provide four cross-sections of the thermal model along selected profiles and along the CROP04 seismic transect[97].

The 3D thermal model highlights that the southeastern Tyrrhenian Sea, including the Aeolian volcanic arc, is characterized by steep thermal gradients, with temperatures reaching approximately 580 °C at depths of

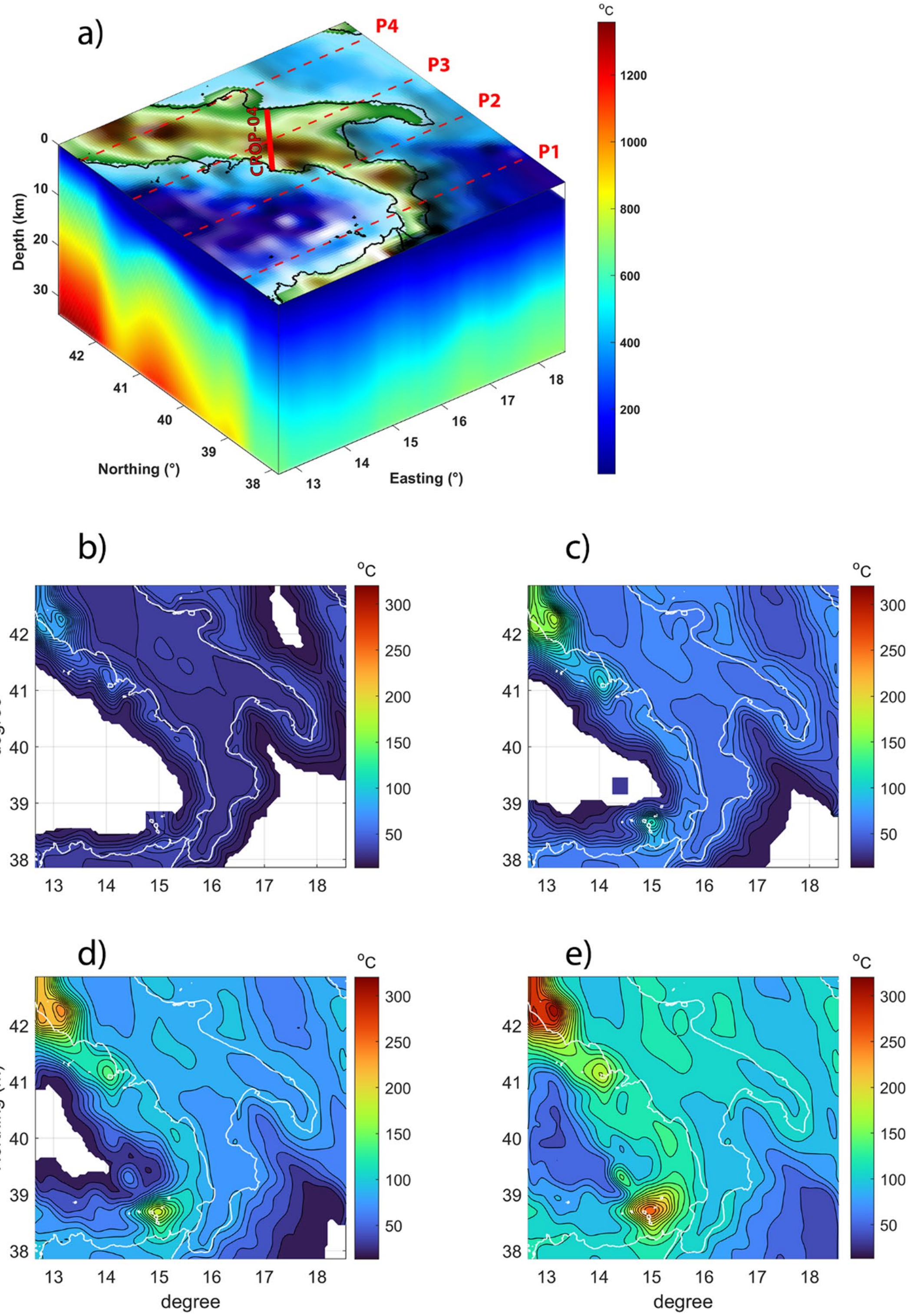

Fig. 10. 3D thermal distribution (**a**) and temperature distributions at 1 km (**b**), 2 km (**c**), 3 km (**d**), and 4 km (**d**) below mean sea level. The profiles are drawn to extract 2D thermal sections. The CROP-04 profile location is shown in (a).

8–10 km. In contrast, similar temperatures are reached at depths of about 33 km beneath the Calabrian Arc and the Apennine fold-and-thrust belt, indicating a much cooler lithosphere. A sharp thermal gradient is observed along the Tyrrhenian coastline.

More specifically, the temperature gradient reduces significantly from around 75 °C/km in the Marsili Basin and Aeolian Arc regions, to roughly 23 °C/km in the Adriatic and Ionian seas, revealing important variability in lateral thermal properties. Regions with high thermal regimes also correspond to remarkably high surface heat flow ($Q_o > 200$ mW/m²)[2,22].

The temperature distribution of the Calabrian arc, Apennines thrust-fold belts and southern end of the Apulian platforms are characterized by low thermal gradients. The predicted Curie depth beneath these areas is estimated to be deep (28–34 km), in agreement with a deep Moho (Fig. 2a) and low surface heat flow values (Fig. 2b). The very high thermal gradient beneath the Tyrrhenian Sea and Aeolian volcanic arcs may be due to asthenospheric uplift (Marsili and Vavilov basins) and subduction-related volcanic activities (e.g., Aeolian volcanic arcs)[37,39],. This is also consistent with the fact that these zones are also characterized by strong positive

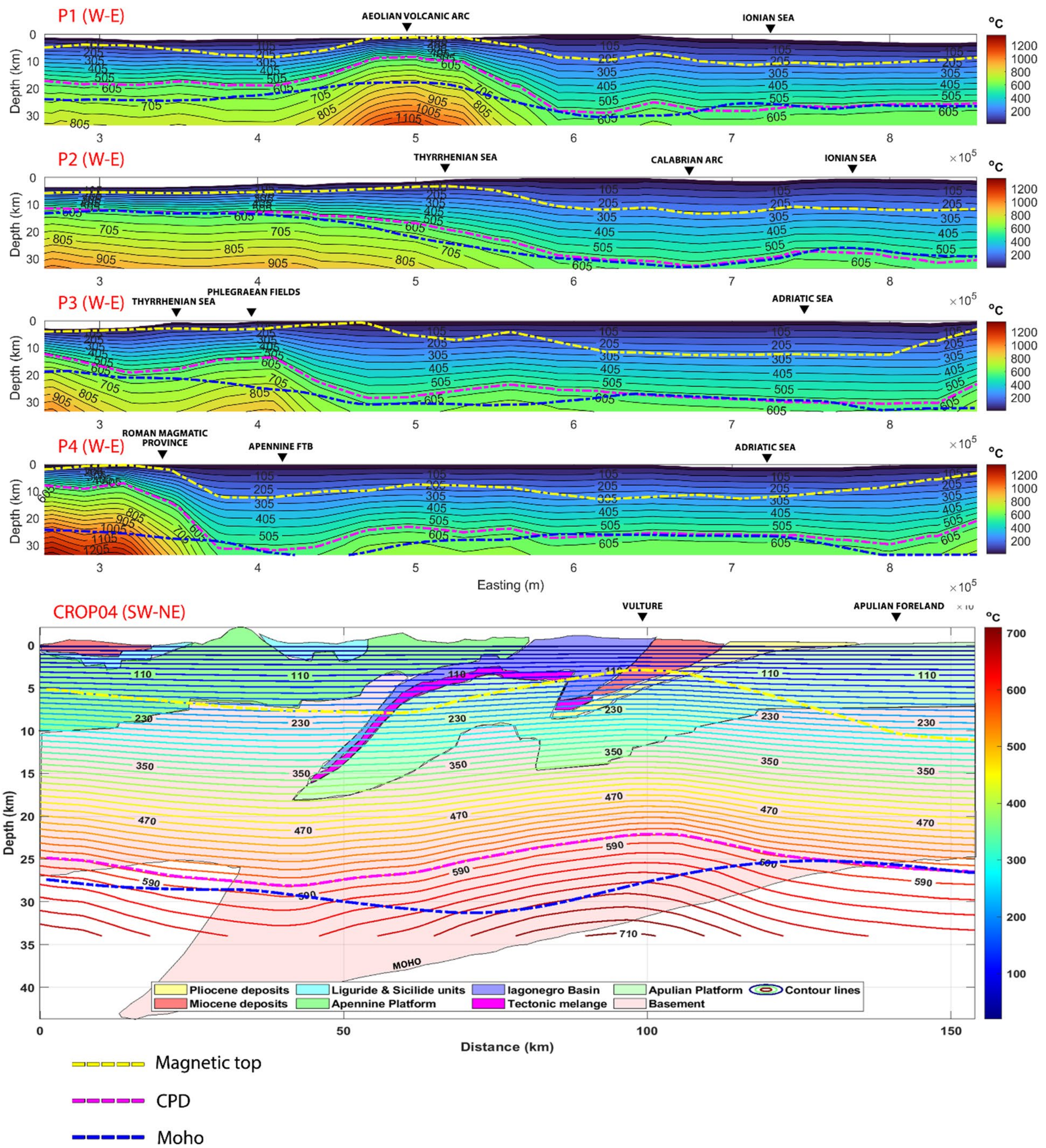

Fig. 11. Vertical sections extracted from the 3D thermal model along the profiles shown in Fig. 4a.

Bouguer gravity anomaly[52,98,99] and thin crust[97]. High temperature gradient (580 °C at approximately 8 km) is found in the regions of the Roman Magmatic Province, decreasing sharply close to the Apennines, where the same temperature is reached at nearly 34 km depth (P4 in Fig. 11). This strong thermal contrast is also evident in the surface heat-flow pattern.

Locally elevated thermal gradients are observed east of Campania, particularly across the Gargano Promontory. Within the Adriatic Sea, the thermal structure exhibits pronounced lateral variability: temperatures of ~ 580 °C are estimated at ~ 25 km depth in the northern Adriatic and at ~ 30 km near the Dinarides (P3 and P4 in Fig. 11). A comparable lateral variability is also evident in surface heat-flow values, potentially reflecting crustal uplift in the northern Adriatic domain.

These elevated gradients likely result from the presence of shallow basement rocks, combined with intense uplift and erosion, as well as localized magmatic activity associated with Mt. Vulture and nearby volcanic systems. Such complexity is consistent with previous studies[56,57,82] which describe the Adriatic region as structurally heterogeneous.

We superimposed the thermal model onto the geological cross-section proposed by Mazzoli et al.[100], constructed along the seismic profile CROP04, in order to provide an integrated and conceptual framework linking temperature distribution with crustal architecture (Fig. 11).

The resulting thermo-structural section highlights significant lateral variations in the depth of isotherms, reflecting the interplay between tectonic setting and thermal regime. In particular, the depth of the ~ 580 °C isotherm is around 25 km beneath the Tyrrhenian margin, indicating a relatively high geothermal gradient consistent with the extensional tectonic domain. Moving eastward beneath the Apennine fold-and-thrust belt, this isotherm deepens to over 28–30 km, suggesting a cooler and thicker crustal sector associated with compressional tectonics and crustal stacking.

Further east, in correspondence with the Mt. Vulture volcanic area and its surroundings, the isotherm rises again to shallower depths (approximately 20 km), likely reflecting localized thermal anomalies linked to magmatic processes or mantle upwelling. Toward the Adriatic foreland, the isotherms progressively deepen once more, indicating a return to lower geothermal gradients and a more thermally stable lithospheric domain.

Overall, the observed geometry of the isotherms mirrors the transition from the Tyrrhenian back-arc extensional system to the Apenninic orogenic belt and finally to the relatively undeformed Adriatic foreland, emphasizing the strong control exerted by tectonic processes on the regional thermal structure.

We have also computed a new surface heat flow map (Fig. 12a). It shows a very high heat flow (about 200 mW/m^2) over the southeastern Tyrrhenian Sea (Aeolian volcanic arcs) and parts of the Roman Magmatic Province, rapidly decreasing toward the Apennines chain. A very low heat flow (about 40 mW/m^2) is observed over the Calabrian arc. An intermediate heat flow (60–80 mW/m^2) is predicted in eastern Campania, Gargano promontory and Adriatic coast. There is a general agreement between our heat flow model and previous heat flow models[2,21,22,23]. Moreover, an overall good match between the observed heat flow and the calculated heat flow is shown in Fig. 12b. In Fig. 12c, we provide a statistical analysis of the heat flow error based on the uncertainty analysis of the Curie depth model. Here we note that large part of the estimated errors range between 2 and 10 mW/m^2, which additionally validates our heat flow model. However, it is important to note that spectral analysis of magnetic data may not be able to detect local anomalies[13] and this could be the reason why there are local very high heat flow values (Fig. 2b) that are not visible in our model.

Discussion and implications

Establishing a temperature model within the lithosphere requires a not easy definition of the deep thermal constraints, of the crustal structure and of the related physical parameter models. Nevertheless, different

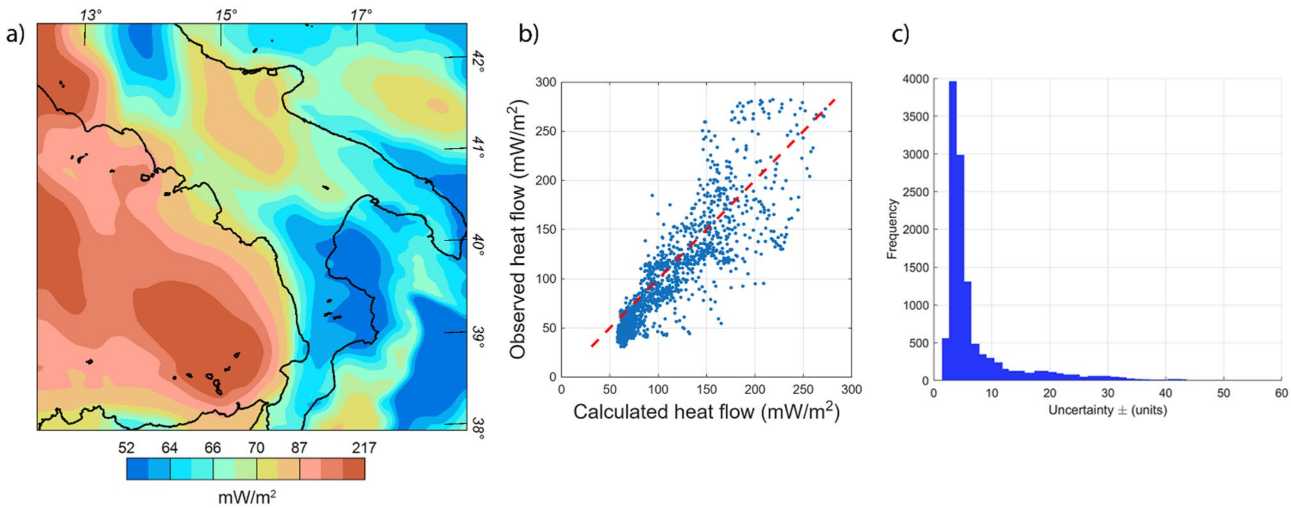

Fig. 12. (**a**) Estimated surface heat flow map, (**b**) comparison between the observed and calculated heat flow and (**c**) histogram of the computed heat flow uncertainty.

geothermal models have been proposed and produced[5,12,22,30,93,101,102]. Several thermal and geochemical analysis have been also carried out to map and characterize the subsurface thermal distributions and evaluate the geothermal potential of the Italian region. As a result, the surface heat flow and shallow temperature distribution of the region is fairly well defined[2,20,26]. However, due to the complex geological setting, existence of volcanic activities, active sedimentation, and ground water circulation, coupled with lack of deep thermal constraints, our understanding of thermal variation is limited at the deep levels.

In our study we attempt to image the 3D thermal distribution beneath Southern Italy using the Curie depth as a main constraint, leading to the definition of the lower boundary condition of the model. The 3D thermal model reveals pronounced lateral and vertical temperature variations across southern Italy, reflecting the strong tectonic segmentation between the Tyrrhenian Sea back-arc domain, the Apennines, and the Adriatic–Ionian foreland. Localized thermal anomalies are predicted where shallow Curie depths coincide with reduced crustal thickness and elevated radiogenic heat production, particularly beneath the Tyrrhenian sector and volcanic provinces. Similar associations between shallow Curie depths, lithospheric thinning, and high geothermal gradients have been documented in other back-arc and extensional settings[1,13,14].

The interpretation of these anomalies must be framed within the assumptions of a steady-state conductive model. Elevated temperatures in the Tyrrhenian domain are directly constrained by shallow Curie isotherms and high modelled heat flow, consistent with asthenospheric upwelling and enhanced mantle heat input inferred from geophysical and geochemical studies[22,30,51]. Conversely, cooler thermal anomalies beneath the Apennine belt and Calabrian Arc correspond to deeper Curie depths, thicker crust, and lower radiogenic heat production, in agreement with previous geothermal and seismic studies[2,18]. However, as discussed in Sect. 1.1, both CPD and Moho depth estimates are affected by uncertainties of the order of ~2–3 km, especially in tectonically complex regions. Consequently, areas where the Curie is slightly deeper than the Moho may fall within the combined uncertainty of the two models and should not be overinterpreted. Nevertheless, where the differences substantially exceed the estimated uncertainty bounds, the presence of a magnetized upper mantle cannot be excluded. One plausible explanation involves mantle serpentinization, a process that promotes the formation of magnetite during hydration of peridotitic rocks and can impart significant magnetization to mantle domains under relatively cold thermal conditions. Such conditions have been independently inferred in the Ionian domain and beneath the Calabrian Arc, where seismic and geological evidence suggests the presence of hydrated or serpentinized mantle[84,85].

However, given the regional scale of the spectral analysis and the intrinsic limitations in resolving sharp vertical contrasts, this interpretation remains tentative. Higher-resolution magnetic data, together with independent seismic and petrological constraints, would be required to robustly discriminate between thermal and compositional controls on mantle magnetization.

Once we define/assume the top boundary conditions from surface data and bottom constraints, the behavior of the geotherm model depends on the heat production and thermal conductivity of the crust. Moreover, integrating deep constraints with near surface thermal data helps to better constrain the shallow thermal distribution. Unfortunately, there are not enough near-surface thermal data to integrate with our model. Nevertheless, we take advantage of very few available near-surface thermal models to compare with our thermal model: Trecase1 (T1), M. Forcuso1 (MF1), Serra S.M. (SSM) and Puglia1 (Pu1) (from Della Vedova et al.[2]).

We show the geotherms constrained by these near-surface thermal models and Curie depth in Fig. 13. The comparison between these two independent approaches highlights both consistencies and local discrepancies in the reconstructed thermal structure.

In several cases, the geotherms derived from shallow thermal data deviate from the CPD-based geotherms, being either higher or lower depending on local conditions. A notable example is represented by the Puglia1 (Pu1) site, where the estimated geotherm is systematically lower than the CPD-constrained profile. This discrepancy can be attributed to the influence of near-surface processes, such as groundwater circulation and sedimentation, which are known to significantly perturb the shallow thermal regime and reduce the apparent geothermal gradient. Alternatively, it may reflect lateral variability in the Curie depth at the local scale, which cannot be fully resolved by spectral methods and may lead to oversimplified CPD estimates.

To account for model uncertainties, we incorporated the error bounds associated with the CPD-derived thermal model, resulting in an uncertainty envelope for each geotherm (grey shaded band in Fig. 13). This uncertainty is relatively limited at shallow depths (approximately 10–20 °C within the upper 10 km), but increases progressively with depth, reaching values on the order of ~80 °C at ~30 km. This trend reflects the intrinsic limitations of Curie depth estimation from spectral analysis, as well as the cumulative effect of uncertainties in thermal properties, boundary conditions, and model assumptions. Furthermore, it is important to note that CPD estimates are inherently sensitive to variations in lithological composition and magnetic mineralogy, which introduce additional, often poorly constrained sources of uncertainty[103]. Despite these limitations, the overall agreement between CPD-based and near-surface-constrained geotherms supports the robustness of the integrated approach and provides valuable insights into the regional thermal structure.

It is also important to note that, in this study, we consider a steady state heat conduction equation model. However, not all the heat may reach the surface by conduction, especially in active regions. Moreover, we used the same equation to compute the thermal distribution beneath the Tyrrhenian Sea and the Apennines. However, in practice, the thermal distribution beneath oceanic crust is generally computed using a half-space cooling model[87,104,105] or a plate cooling model[87,102]. However, the importance of deriving the Curie depth from magnetic data lies in the fact that it provides an estimate of the temperature at depth even in non-stationary situations[74].

It is clear from the thermal model that there are strong lateral and vertical thermal variations between the Tyrrhenian Sea, the Apennines and the Ionian and Adriatic Sea. It is worth noting that there are local very high heat flow values over the Aeolian volcanic arcs and Marsili basin (> 250 mW/m^2)[2] and deriving geotherm

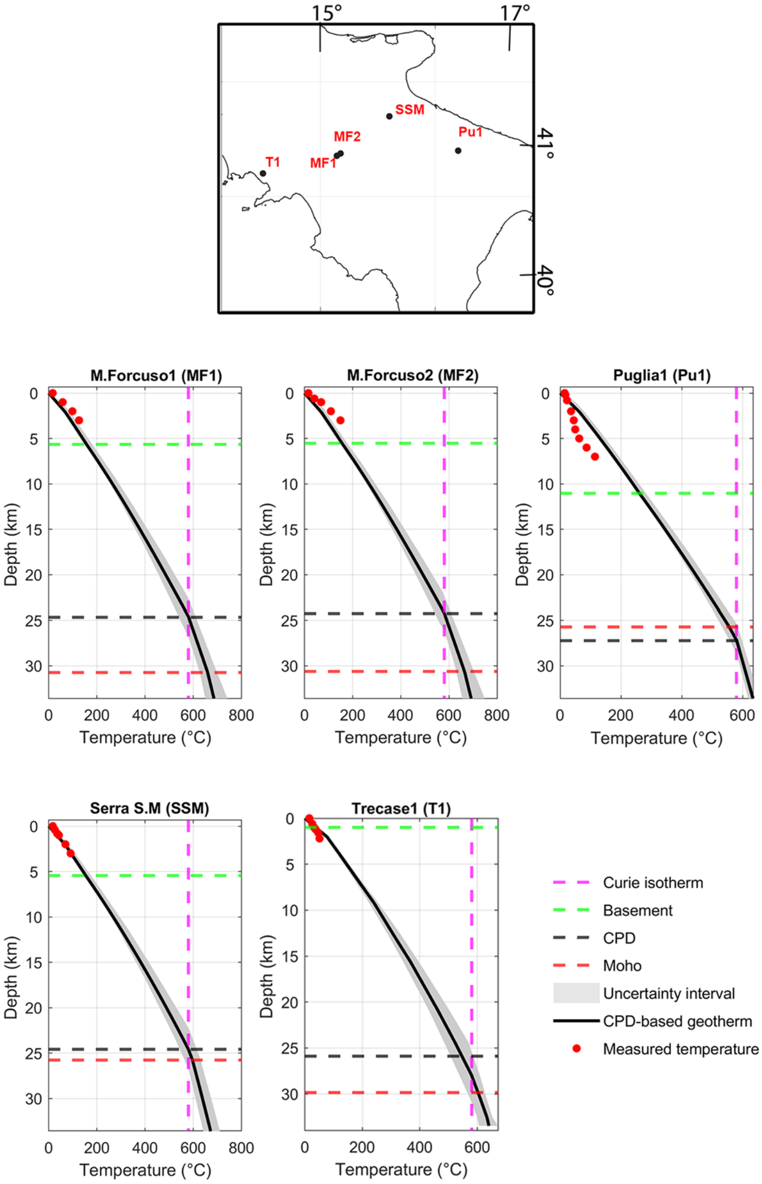

Fig. 13. Geotherms based on near-surface thermal data (red dots) and Curie isotherm-based geotherms (black line). Red dots reproduced from Della Vedova et al.[2]. Location of boreholes is also shown.

models using these very high heat flow values may lead to higher geotherm values than our model. Moreover, the interface between the upper and lower mantle in the Tyrrhenian Sea is not indicated in our crustal model, where the lithosphere - asthenosphere boundary (LAB) is expected to vary from 1100 to 1400 °C[22,30,101,102,106]. A value of about 1330 °C is used in most studies. Since our main focus in this study is on the Curie isotherm, which is significantly shallower than the LAB, there may be some uncertainty in the Tyrrhenian Sea where there is the LAB interface.

Nevertheless, our results are broadly consistent with the lithospheric-scale framework recently proposed by Zhang et al.[57], who investigated the thermochemical structure of the Western–Central Mediterranean lithosphere using integrated geophysical–geochemical modeling. The spatial variation of Curie depths and geothermal gradients obtained in this study mostly reflects similar large-scale thermal segmentation. In is important to note that, while Zhang et al.[57] provide a regional geodynamic framework linking slab rollback, mantle flow, and lithospheric architecture along a 2D transect, our study is more focused in interpreting the shallow thermal structure of the crust and in quantifying the 3D spatial distribution of geothermal gradients and Curie isotherm depths across Southern Italy.

Processes such as uplift, erosion, magmatic intrusions, or advective heat transport may locally perturb the thermal field, as documented in volcanic and hydrothermal areas of southern Italy[20,25,26]. In the Adriatic region, for instance, Zhang et al.[56,57] highlight the intricate architecture of the Adria microplate, which differs significantly from adjacent plates. They report average crustal densities of ~2,830 kg/m³ and substantial crustal thickening beneath the External Dinarides (up to 45–50 km), interpreted as the result of maximum plate bending. A complementary perspective is offered by Faccenna et al.[80], who interpret the Puglia uplift as a consequence of buckling within a thick continental lithosphere in the foreland of the Apenninic subduction system. Marra et al.[107] similarly support an uplift component, though they attribute it to broader lithospheric-scale processes. Baccheschi et al.[108] introduce a deeper geodynamic mechanism, identifying belt-perpendicular fast seismic anisotropy axes in the Gargano region. These are interpreted as evidence of shallow mantle flow through a narrow horizontal tear in the Ionian slab, suggesting that the observed lateral variability is not purely crustal but linked to slab fragmentation at depth.

Importantly, there is some divergence regarding the net topographic expression of these processes. Zhang et al.[56,57] argue that the Adriatic microplate is overall characterized by subsidence: the combination of thick lithosphere and adjacent subducting slabs exerts a downward pull, maintaining the region below sea level. In this framework, localized uplift at Gargano represents an anomalous feature within a broader foreland basin setting.

While this study attributes elevated thermal gradients primarily to shallow basement conditions and uplift-related processes, Zhang et al.[56,57] instead emphasize the role of a three-layered crystalline crust with increasing density at depth (up to ~ 3,080 kg/m³ in the lower crust), which they use to explain regional gravity and geoid anomalies rather than localized thermal variations. Therefore, we interpret uplift and shallow basement rocks as the primary controls on the observed thermal anomalies, whereas other studies[107,108], invoke deeper geodynamic processes, such as mantle flow, slab tearing, and lithospheric buckling, to explain the same regional complexity.

Our model demonstrates that the first-order thermal anomalies at regional scale can be explained without invoking transient or advective processes, relying solely on variations in Curie depth, crustal architecture, and internal heat production. This distinction highlights the role of deep lithospheric structure as the primary control on the regional geothermal framework.

Beyond temperature distribution, the modelled thermal field provides quantitative constraints on the mechanical behaviour of the lithosphere. Experimental and theoretical studies indicate that temperatures of approximately 350–450 °C correspond to the brittle–ductile transition in the continental crust, marking a sharp reduction in effective strength and viscosity[109,110]. In the Tyrrhenian domain, these temperatures are reached at shallow depths (< 10–12 km), implying a thin brittle crust and a mechanically weak lithosphere.

Such thermal weakening is consistent with the observed extensional tectonics, high seismic attenuation, and widespread Quaternary volcanism in the Tyrrhenian region[51,111]. In contrast, beneath the Apennine belt and the Adriatic–Ionian foreland, equivalent temperatures are reached at significantly greater depths (> 25–30 km), implying a thicker brittle layer and a mechanically stronger lithosphere. This rheological contrast supports interpretations of strain localization in the hot back-arc domain and more distributed or rigid deformation within the colder orogenic belt, in agreement with thermo-mechanical models of the central Mediterranean[24,25]. Although crustal viscosity and strength are not explicitly parameterized in the present model, the predicted temperature field places robust first-order bounds on lithospheric rheology and deformation style.

To evaluate the predictive capability of the model, the inferred surface heat-flow values were quantitatively compared with published heat-flow datasets for Italy[2,21,22]. At regional scale, the model successfully reproduces the major thermal provinces of southern Italy, including high heat-flow values (> 150–200 mW m^{-2}) in the Tyrrhenian domain and low values (< 50 mW m^{-2}) beneath the Apennine belt and Calabrian Arc.

A point-by-point comparison indicates that most modeled values fall within ± 20–30 mW m^{-2} of observed measurements, comparable to the uncertainty range of heat-flow determinations themselves[19,30]. Larger discrepancies are primarily associated with areas affected by active hydrothermal circulation or recent volcanism, such as volcanic islands and coastal geothermal fields, where advective heat transport plays a dominant role[20,26]. Another source of discrepancy is the spatial resolution. The results inferred from spectral analysis are valid at scales of tens of kilometres, which inhibits a full comparison with local-scale wells information. Nevertheless, these results confirm that the model reliably predicts the regional background conductive heat-flow field, rather than localized anomalies controlled by shallow processes.

Conclusions

The Curie depth constraint allowed us to better image the thermal distribution beneath the complex geological settings of the southern Italian peninsula, where significant lateral and vertical thermal variations over short distance are observed. Another major advantage is that the Curie depth acts as an important constraint, especially where there is no or insufficient surface heat flow data, thanks to the regional coverage of magnetic data. Moreover, the Curie depth can be used to constrain basin modeling, which is useful to understand the maturation history of organic materials.

The curvature of the geothermal gradient depends on the heat source and thermal conductivity of the crust. This is why we integrated near surface thermal data with the Curie depth, to better define the thermal parameters (heat production and thermal conductivity) within the crust, which in turn is useful to better constrain the geotherm models.

The thermal model indicates substantial spatial variability in the lithospheric heat regime, characterized by a progressive westward rise in geothermal gradient from the Adriatic and Ionian sectors toward the Tyrrhenian Sea. Elevated gradients are concentrated in zones of back-arc extension and asthenospheric upwelling beneath the Vavilov and Marsili basins, and in areas influenced by subduction-driven magmatism along the Aeolian arc.

Areas marked by elevated temperatures and high heat-flow values, such as the Tyrrhenian sector, the eastern margin of the Adriatic, and the Roman Magmatic Province, emerge as particularly favorable prospects for geothermal resource development.

In this study we neglected the effects of convective and advective systems. However, these heat transfer mechanisms may locally play an important role, especially beneath the Tyrrhenian region and thus the model can be further refined by incorporating these heat transfer mechanisms.

By anchoring the thermal structure to Curie isotherm geometry derived from magnetic data, the model reduces uncertainty in basal boundary conditions and enables consistent comparison across distinct tectonic domains.

The added value of this approach lies not in redefining known surface heat-flow patterns, but in demonstrating that these patterns arise naturally from the deep lithospheric thermal architecture of Southern Italy. This strengthens interpretations of geothermal gradients, provides new quantitative constraints on lithospheric rheology, and establishes a robust baseline for future coupled thermo-mechanical or hydrothermal investigations.

Data availability

The maps of the Moho depth, CPD and magnetic depth to the top, used for the thermal modeling of Southern Apennines are available at Kelemework et al.[112].

Received: 2 December 2025; Accepted: 8 May 2026
Published online: 25 May 2026

References

1. Artemieva, I. M. & Mooney, W. D. Thermal thickness and evolution of Precambrian lithosphere: A global study. *J. Geophys. Res.* https://doi.org/10.1029/2000JB900439 (2001).
2. Della Vedova, B., Bellani, S., Pellis, G. & Squarci, P. Deep temperatures and surface heat flow distribution. In *Anatomy of an Orogen: the Apennines and Adjacent Mediterranean Basins* (eds Vai, G. B. & Martini, I. P.) 65–76 (Springer Netherlands, 2001).
3. Pasquale, V., Verdoya, M. & Chiozzi, P. *Geothermics: Heat Flow in the Lithosphere* (Springer International Publishing, 2014).
4. Montanari, D. et al. Geothermal resources within carbonate reservoirs in western Sicily (Italy): A review. *Earth-Sci. Rev.* **169**, 180–201 (2017).
5. Čermák, V. & Bodri, L. Two-dimensional temperature modelling along five East-European geotraverses. *J. Geodyn.* **5**, 133–163 (1986).
6. Chen, L. et al. Seismically constrained thermo-rheological structure of the eastern Tibetan margin: Implication for lithospheric delamination. *Tectonophysics* **627**, 122–134 (2014).
7. Fuchs, S. et al. A new database structure for the IHFC Global Heat Flow Database. *ijthfa* **4**, 1–14 (2021).
8. Berntsson, F., Lin, C., Xu, T. & Wokiyi, D. An efficient regularization method for a large scale ill-posed geothermal problem. *Comput. Geosci.* **105**, 1–9 (2017).
9. Currie, C. A. & Hyndman, R. D. The thermal structure of subduction zone back arcs. *J. Geophys. Res.* https://doi.org/10.1029/2005JB004024 (2006).
10. Artemieva, I. *The Lithosphere: An Interdisciplinary Approach* (Cambridge University Press, 2011).
11. Chapman, D. S. Thermal gradients in the continental crust. *Geol. Soc. Lond. Special Publications*. **24**, 63–70 (1986).
12. Hasterok, D. & Chapman, D. S. Heat production and geotherms for the continental lithosphere. *Earth Planet. Sci. Lett.* **307**, 59–70 (2011).
13. Tanaka, A., Okubo, Y. & Matsubayashi, O. Curie point depth based on spectrum analysis of the magnetic anomaly data in East and Southeast Asia. *Tectonophysics* **306**, 461–470 (1999).
14. Bouligand, C., Glen, J. M. G. & Blakely, R. J. Mapping Curie temperature depth in the western United States with a fractal model for crustal magnetization. *J. Geophys. Res.* **114**, 21,823 (2009).
15. Kelemework, Y., Fedi, M. & Milano, M. A review on spectral analysis of magnetic data for depth estimation. *Geophysics* https://doi.org/10.1190/geo2020-0268.1 (2021).
16. Gard, M. & Hasterok, D. A global Curie depth model utilising the equivalent source magnetic dipole method. *Phys. Earth Planet. Inter*. **313**, 106672 (2021).
17. Toksoz, N. M., Li, Y. & Lee, J. M. Seismic imaging of fractures in geothermal reservoirs. in *IECEC 96. Proceedings of the 31st Intersociety Energy Conversion Engineering Conference* vol. 3 1647–1652 vol.3 (1996).
18. Tumanian, M., Frezzotti, M. L., Peccerillo, A., Brandmayr, E. & Panza, G. F. Thermal structure of the shallow upper mantle beneath Italy and neighbouring areas: Correlation with magmatic activity and geodynamic significance. *Earth-Sci. Rev.* **114**, 369–385 (2012).
19. Beardsmore, G. R. & Cull, J. P. *Crustal Heat Flow: A Guide to Measurement and Modelling* (Cambridge University Press, 2001).
20. Cataldi, R. et al. Geothermal ranking of Italian territory. *Geothermics* vol. 24 115–129 Preprint at (1995). https://doi.org/10.1016/0375-6505(94)00026-9
21. Pasquale, V., Verdoya, M. & Chiozzi, P. Thermal state and deep earthquakes in the Southern Tyrrhenian. *Tectonophysics* **306**, 435–448 (1999).
22. Zito, G., Mongelli, F., de Lorenzo, S. & Doglioni, C. Heat flow and geodynamics in the Tyrrhenian Sea. *Terra Nova*. **15**, 425–432 (2003).
23. Trumpy, E. & Manzella, A. Geothopica and the interactive analysis and visualization of the updated Italian National Geothermal Database. *Int. J. Appl. Earth Obs Geoinf.* **54**, 28–37 (2017).
24. Solaro, G., Tizzani, P., Milano, G. & Pauselli, C. Rheological behaviour of the crust in Southern Apennine (Italy): Results from a thermal and seismological study. *Terra Nova* **19**, 353–359 (2007).
25. Castaldo, R. et al. The role of thermo-rheological properties of the crust beneath Ischia Island (Southern Italy) in the modulation of the ground deformation pattern. *J. Volcanol. Geotherm. Res.* **344**, 154–173 (2017).
26. Minissale, A., Donato, A., Procesi, M., Pizzino, L. & Giammanco, S. Systematic review of geochemical data from thermal springs, gas vents and fumaroles of Southern Italy for geothermal favourability mapping. *Earth-Sci. Rev.* **188**, 514–535 (2019).
27. Floridia, G., Cacace, M., Scheck-Wenderoth, M., Bott, J. & Viccaro, M. 3D thermal model of Sicily (Southern Italy) and perspectives for new exploration campaigns for geothermal resources. *Glob. Planet. Change* **218**, 103976 (2022).
28. Giuffrida, M., Floridia, G., Cacace, M. & Viccaro, M. Thermal model of the Pantelleria Island (Sicily Channel, Southern Italy): New insights for promoting the sustainable exploitation of geothermal resources on the island. *Geotherm. Energy* https://doi.org/10.1186/s40517-025-00340-x (2025).
29. Vespasiano, G. et al. Three-dimensional lithospheric-scale thermal model as supporting tool for new exploration campaigns for geothermal resources: Insights from the Calabria region (Southern Italy). *Geothermics* **136**, 103604 (2026).
30. Mongelli, F., Zito, G., De Lorenzo, S. & Doglioni, C. Geodynamic interpretation of the heat flow in the Tyrrhenian Sea. *to Deep Mantle: Architecture of the* … (2004).
31. Mather, B. & Fullea, J. Constraining the geotherm beneath the British Isles from Bayesian inversion of Curie depth: Integrated modelling of magnetic, geothermal, and seismic data. *Solid Earth* **10**, 839–850 (2019).
32. Guerrero-Martínez, F. J., Prol-Ledesma, R. M., Carrillo-De La Cruz, J. L., Rodríguez-Díaz, A. A. & González-Romo, I. A. A three-dimensional temperature model of the Acoculco caldera complex, Puebla, Mexico, from the Curie isotherm as a boundary condition. *Geothermics* **86**, 101794 (2020).

33. Blakely, R. J. Curie temperature isotherm analysis and tectonic implications of aeromagnetic data from Nevada. *J. Geophys. Res.* **93**, 11817 (1988).
34. Ross, H. E., Blakely, R. J. & Zoback, M. D. Testing the use of aeromagnetic data for the determination of Curie depth in California. *Geophysics* **71**, L51–L59 (2006).
35. Abraham, E. M. et al. Spectral analysis of aeromagnetic data for geothermal energy investigation of Ikogosi Warm Spring - Ekiti State, southwestern Nigeria. *Geotherm. Energy* 6 (2014).
36. Critelli, S. & Le Pera, E. Detrital modes and provenance of Miocene sandstones and modern sands to the Southern Apennines thrust-top basins (Italy). *J. Sediment. Res.* 824–835 (1994).
37. Cello, G. & Mazzoli, S. Apennine tectonics in southern Italy: A review. *J. Geodyn.* **27**, 191–211 (1998).
38. Castellarin, A. & Cantelli, L. Geology and evolution of the Northern Adriatic structural triangle between Alps and Apennine. *Rend. Lincei Sci. Fis. Nat.* **21**, 3–14 (2010).
39. Patacca, E. & Scandone, P. Geological interpretation of the CROP-04 seismic line (Southern Apennines, Italy). *Boll. Soc. Geol. Ital* 297–315 (2007).
40. Patacca, E., Scandone, P., Di Luzio, E., Cavinato, G. P. & Parotto, M. Structural architecture of the Central Apennines: Interpretation of the CROP 11 seismic profile from the Adriatic coast to the orographic divide. *Tectonics* https://doi.org/10.1029/2005TC001917 (2008).
41. Scrocca, D. Southern Apennines: structural setting and tectonic evolution. *J virtual explor* **36**, n/a-n/a (2010).
42. Vezzani, L., Festa, A. & Ghisetti, F. C. *Geology and Tectonic Evolution of the Central-Southern Apennines, Italy* (Geological Society of America, 2010).
43. Cosentino, D., Cipollari, P., Marsili, P. & Scrocca, D. Geology of the Central Apennines: A regional review. *Journal Virtual Explorer* **36**, 1–37 (2010).
44. Fellin, M. G. et al. Transition from slab roll-back to slab break-off in the Central Apennines, Italy: Constraints from the stratigraphic and thermochronologic record. *Geol. Soc. Am. Bull.* 1916–1930 (2022).
45. Ghisetti, F. & Vezzani, L. Interfering paths of deformation and development of arcs in the fold-and-thrust belt of the Central Apennines (Italy). *Tectonics* 523–536 (1997).
46. Cavazza, W., Roure, F. & Ziegler, P. A. The Mediterranean Area and the Surrounding Regions: Active Processes, Remnants of Former Tethyan Oceans and Related Thrust Belts In (eds Cavazza, W. et al.) (2004).
47. Doglioni, C., Harabaglia, P., Martinelli, G., Mongelli, F. & Zito, G. A geodynamic model of the Southern Apennines accretionary prism. *Terra Nova* **8**, 540–547 (1996).
48. Casero, P. et al. Neogene geodynamic evolution of the Southern Apennines. *Memorie della Soc. Geologica Italiana*. **41**, 109–120 (1988).
49. Patacca, E., Sartori, R. & Scandone, P. Tyrrhenian basin and Apenninic arcs: Kinematic relations since Late Tortonian times. *Memorie della Soc. Geologica Italiana*. **45**, 425–451 (1990).
50. Mazzoli, S. et al. Tectonic burial and young (< 10 Ma) exhumation in the southern Apennines fold-and-thrust belt (Italy). *Geology* **36**, 243–246 (2008).
51. Sartori, R. The Tyrrhenian back-arc basin and subduction of the Ionian lithosphere. *Episodes* **26**, 217–221 (2003).
52. Barone, A., Milano, M. & Fedi, M. Inhomogeneous magnetization of Tyrrhenian seamounts revealed from gravity and magnetic correlation analysis. *J. Geophys. Res. Solid Earth* **129**, e2024JB028977 (2024).
53. Milia, A., Torrente, M. M. & Iannace, P. Pliocene-Quaternary orogenic systems in Central Mediterranean: The Apulia-Southern Apennines-Tyrrhenian Sea example: Pliocene-Quaternary orogenic systems. *Tectonics* **36**, 1614–1632 (2017).
54. Bosellini, A. Outline of the Geology of Italy. In *Landscapes and Landforms of Italy* (eds Soldati, M. & Marchetti, M.) 21–27 (Springer International Publishing, 2017).
55. Kelemework, Y. et al. Crustal structure in the Campanian region (Southern Apennines, Italy) from potential field modelling. *Sci. Rep.* **11**, 14510 (2021).
56. Zhang, W. et al. Geophysical-petrological model for bidirectional mantle delamination of the Adria Microplate beneath the Northern Apennines and Dinarides orogenic systems. *J. Geophys. Res. Solid Earth.* **127**, 7722–7743 (2022).
57. Zhang, W. et al. The lithosphere and upper mantle of the western-central Mediterranean region from integrated geophysical-geochemical modeling. *J Geophys. Res. Solid Earth* **129**, e2023JB028435 (2024).
58. Marani, M. P. & Trua, T. Thermal constriction and slab tearing at the origin of a superinflated spreading ridge: Marsili volcano (Tyrrhenian Sea): Superinflated spreading ridge. *J. Geophys. Res.* **107**, EPM 3-1-EPM 3-15 (2002).
59. Faccenna, C., Piromallo, C., Crespo-Blanc, A., Jolivet, L. & Rossetti, F. Lateral slab deformation and the origin of the western Mediterranean arcs: Arcs of the mediterranean. *Tectonics* 23, (2004).
60. Carlino, S. Heat flow and geothermal gradients of the Campania region (Southern Italy) and their relationship to volcanism and tectonics. *J. Volcanol. Geotherm. Res.* **365**, 23–37 (2018).
61. Frondini, F., Cardellini, C., Caliro, S., Chiodini, G. & Morgantini, N. Regional groundwater flow and interactions with deep fluids in Western Apennine: The case of Narni-Amelia Chain (Central Italy): Regional groundwater flow and interactions with deep fluids. *Geofluids* **12**, 182–196 (2012).
62. Gambardella, B. et al. Fluxes of deep CO2 in the volcanic areas of central-southern Italy. *J. Volcanol Geotherm. Res.* **136**, 31–52 (2004).
63. Chiodini, G., Cardellini, C., Caliro, S., Chiarabba, C. & Frondini, F. Advective heat transport associated with regional Earth degassing in Central Apennine (Italy). *Earth Planet. Sci. Lett.* **373**, 65–74 (2013).
64. Frondini, F. et al. Measuring and interpreting CO_2 fluxes at regional scale: the case of the Apennines, Italy. *J. Geol. Soc. Lond.* **176**, 408–416 (2019).
65. Spector, A. & Grant, F. S. Statistical models for interpreting aeromagnetic data. *Geophysics* **35**, 293–302 (1970).
66. Fedi, M., Quarta, T. & De Santis, A. Inherent power-law behavior of magnetic field power spectra from a Spector and Grant ensemble. *Geophysics* **62**, 1143–1150 (1997).
67. Blakely, R. J. *Potential Theory in Gravity and Magnetic Applications* (Cambridge University Press, 1996).
68. Maus, S., Gordon, D. & Fairhead, D. Curie-temperature depth estimation using a self-similar magnetization model. *Geophys. J. Int.* **129**, 163–168 (1997).
69. Bansal, A. R., Gabriel, G., Dimri, V. P. & Krawczyk, C. M. Estimation of depth to the bottom of magnetic sources by a modified centroid method for fractal distribution of sources: An application to aeromagnetic data in Germany. *Geophysics* **76**, L11–L22 (2011).
70. Shuey, R. T., Schellinger, D. K., Tripp, A. C. & Alley, L. B. Curie depth determination from aeromagnetic spectra. *Geophys. J. Int.* **50**, 75–101 (1977).
71. Connard, G., Couch, R. & Gemperle, M. Analysis of aeromagnetic measurements from the Cascade Range in central Oregon. *Geophysics* **48**, 376–390 (1983).
72. Li, C.-F., Wang, J., Lin, J. & Wang, T. Thermal evolution of the North Atlantic lithosphere: New constraints from magnetic anomaly inversion with a fractal magnetization model: North Atlantic Curie depths. *Geochem. Geophys. Geosyst.* **14**, 5078–5105 (2013).
73. Ravat, D., Pignatelli, A., Nicolosi, I. & Chiappini, M. A study of spectral methods of estimating the depth to the bottom of magnetic sources from near-surface magnetic anomaly data. *Geophys. J. Int.* **169**, 421–434 (2007).

74. Salem, A. et al. Depth to Curie temperature across the central Red Sea from magnetic data using the de-fractal method. *Tectonophysics* **624–625**, 75–86 (2014).
75. AGIP. Carta Aeromagnetica d'Italia (scala 1:500.000). (1981).
76. Chiappini, M. et al. Shaded relief magnetic anomaly map of Italy and surrounding marine areas. *Annals Geophysics* **43**, 983–989 (2000).
77. Milano, M., Fedi, M. & Fairhead, J. D. The deep crust beneath the Trans-European Suture Zone from a multiscale magnetic model: MULTISCALE MAGNETIC MODEL OF THE TESZ. *J. Geophys. Res. [Solid Earth]*. **121**, 6276–6292 (2016).
78. Ridsdill-Smith, T. A. The Application of the Wavelet Transform to the Processing of Aeromagnetic Data. (University of Western Australia.).
79. Finetti, I. Structure, stratigraphy and evolution of Central Mediterranean. *Boll. Geofis. Teor. Appl.* **XIV**, 247–312 (1982).
80. Faccenna, C. et al. Mantle dynamics in the Mediterranean. *Rev. Geophys.* **52**, 283–332 (2014).
81. van Hinsbergen, D. J. J. et al. Orogenic architecture of the Mediterranean region and kinematic reconstruction of its tectonic evolution since the Triassic. *Gondwana Res.* **81**, 79–229 (2020).
82. Rappisi, F., VanderBeek, B. P., Faccenda, M., Morelli, A. & Molinari I. 3D anisotropic P-wave tomography of the Central Mediterranean: new insights into slab geometry and upper mantle flow patterns. (2022). https://doi.org/10.5194/egusphere-egu22-8102
83. Jolivet, L. Tethys and Apulia (Adria), 100 years of reconstructions. *C R Geosci.* **355**, 9–28 (2024).
84. D'Alessandro, A., Mangano, G., D'Anna, G. & Scudero, S. Evidence for serpentinization of the Ionian upper mantle from simultaneous inversion of P- and S-wave arrival times. *J. Geodyn.* **102**, 115–120 (2016).
85. Polonia, A. et al. Lower plate serpentinite diapirism in the Calabrian Arc subduction complex. *Nat. Commun.* **8**, 2172 (2017).
86. Gola, G. et al. A novel multidisciplinary approach for the thermo-rheological study of volcanic areas: The case study of Long Valley caldera. *J. Geophys. Res. Solid Earth* https://doi.org/10.1029/2020JB020331 (2021).
87. Turcotte, D. L., Schubert, G. & Geodynamics Cambridge University Press, Cambridge, 423 p. (2014).
88. LeVeque, R. J. *Finite Difference Methods for Ordinary and Partial Differential Equations: Steady-State and Time-Dependent Problems*. 329–341Society for Industrial and Applied Mathematics, (2007).
89. Li, Z., Qiao, Z. & Tang, T. *Numerical Solution of Differential Equations: Introduction to Finite Difference and Finite Element Methods* (Cambridge University Press, 2017).
90. Saad, Y. *Iterative Methods for Sparse Linear Systems*. 495–528Society for Industrial and Applied Mathematics, (2003).
91. McAliley, W. A. & Li, Y. Methods to invert temperature data and heat flow data for thermal conductivity in steady-state conductive regimes. *Geosciences* https://doi.org/10.3390/GEOSCIENCES9070293 (2019).
92. Saad, Y. & Schultz, M. H. GMRES: A generalized minimal residual algorithm for solving nonsymmetric linear systems. *SIAM J. Sci. Stat. Comput.* **7**, 856–869 (1986).
93. Furlong, K. P. & Chapman, D. S. Heat flow, heat generation, and the thermal state of the lithosphere. *Annu. Rev. Earth Planet. Sci.* **41**, 385–410 (2013).
94. Vosteen, H.-D. & Schellschmidt, R. Influence of temperature on thermal conductivity, thermal capacity and thermal diffusivity for different types of rock. *Physics and Chemistry of the Earth, Parts A/B/C* **28**, 499–509 (2003).
95. AGIP. Aggiornamenti temperature sotterranee–Pozzi a terra–Esplorazione Geotermica. (1986).
96. Santini, S. et al. Controls of radiogenic heat and Moho geometry on the thermal setting of the Marche region (central Italy): An analytical 3D geothermal model. *Energies* https://doi.org/10.3390/en14206511 (2021).
97. Finetti, I. R. *CROP Project: Deep Seismic Exploration of the Central Mediterranean and Italy* (Elsevier, 2005).
98. Cella, F. et al. Temperature and density of the Tyrrhenian lithosphere and slab and new interpretation of gravity field in the Tyrrhenian Basin. *Tectonophysics* **412**, 27–47 (2006).
99. Cella, F. et al. A review of the gravity and magnetic studies in the Tyrrhenian Basin and its volcanic districts. *Ann. Geophys.* https://doi.org/10.4401/ag-3035 (2008).
100. Mazzoli, S., Ascione, A., Candela, S., Iannace, A. & Vitale, S. Subduction and continental collision events in the southern Apennines: Constraints from two crustal cross-sections. *Rend. Online Soc. Geologica Italiana*. **25**, 78–84 (2013).
101. Pollack, H. N., Sass, J. H. & Stromeyer, D. Crust and Mantle Geothermics In (eds Haenel, R. et al.) (1988).
102. McKenzie, D., Jackson, J. & Priestley, K. Thermal structure of oceanic and continental lithosphere. *Earth Planet. Sci. Lett.* **233**, 337–349 (2005).
103. Stål, T. et al. Properties and biases of the global heat flow compilation. *Front Earth Sci* **10**, 963525 (2022).
104. Turcotte, D. L. & Oxburgh, E. R. Finite amplitude convective cells and continental drift. *J. Fluid Mech.* **28**, 29–42 (1967).
105. Cardoso, R. R. & Hamza, V. M. Finite Half pace model of oceanic lithosphere. *Horizons Earth Sci. Res. edited by: Veress B Szigethy J.* **11**, 375–395 (2011).
106. Pollack, H. N., Hurter, S. J. & Johnson, J. R. Heat flow from the Earth's interior: Analysis of the global data set. *Rev. Geophys.* **31**, 267–280 (1993).
107. Marra, F. et al. The Volsci Volcanic Field (central Italy): Eruptive history, magma system and implications on continental subduction processes. *Geol. Rundsch.* **110**, 689–718 (2021).
108. Baccheschi, P., Confal, J. M. & Pondrelli, S. Splitting intensity tomography to image depth-dependent seismic anisotropy patterns beneath the Italian Peninsula and surrounding regions. *Earth Planet. Sci. Lett.* **646**, 119005 (2024).
109. Ranalli, G. *Rheology of the Earth* (Chapman and Hall, 1995).
110. Bürgmann, R. & Dresen, G. Rheology of the lower crust and upper mantle: Evidence from rock mechanics, geodesy, and field observations. *Annu. Rev. Earth Planet. Sci.* **36**, 531–567 (2008).
111. Carminati, E., Lustrino, M. & Doglioni, C. Geodynamic evolution of the central and western Mediterranean: Tectonics vs. igneous petrology constraints. *Tectonophysics* **579**, 173–192 (2012).
112. Kelemework, Y., Milano, Maurizio, Iorio, M., Abbas, M. A., Fedi, M. & 3D Geothermal Model of the Southern Italian Region based on the Curie Isotherm Depth. *3D Geothermal Model of the Southern Italian Region based on the Curie Isotherm Depth* (2025). https://doi.org/10.5281/zenodo.15636028

Acknowledgements
We thank the two anonymous Reviewers for their thoughtful inputs to our manuscript.

Author contributions
All authors discussed the data, their processing and the models, co-wrote and reviewed the manuscript. M.M., Y.K and M.A.A. conducted the data analysis and built the figures. Y.K. performed the spectral analysis. M.I. collected wells data and contributed to the geological interpretations. M.F. supervised the team.

Funding
This work was part of the project, "Modellazione dell' isoterma di Curie con metodi spettrali per studi geotermici" conducted at the University of Naples Federico II, funded by Eni, and " PRIN 2022 PNRR – TRHAM: relation

between 3D Thermo-Rheological model and seismic hAzard for Risk Mitigation in the urban areas of southern italy", CUP E53D23022000001.

Declarations

Competing interests
The authors declare no competing interests.

Additional information
Correspondence and requests for materials should be addressed to M.M.